Ultrasound-assisted electrodeposition of thin Nickel-based composite coatings with lubricant particles

Tudela-Montes, I, Zhang, Y, Pal, M, Kerr, I & Cobley, AJ

Original citation & hyperlink:
Tudela-Montes, I, Zhang, Y, Pal, M, Kerr, I & Cobley, AJ 2015, 'Ultrasound-assisted electrodeposition of thin Nickel-based composite coatings with lubricant particles' *Surface and Coatings Technology*, vol 276, pp. 89-105
https://dx.doi.org/10.1016/j.surfcoat.2015.06.030

DOI 10.1016/j.surfcoat.2015.06.030
ISSN 0257-8972
ESSN 1879-3347

Publisher: Elsevier

ULTRASOUND-ASSISTED ELECTRODEPOSITION OF THIN NICKEL-BASED COMPOSITE COATINGS WITH LUBRICANT PARTICLES

*IGNACIO TUDELA[1,2 *], YI ZHANG[1], MADAN PAL[1], IAN KERR[1] AND ANDREW J. COBLEY[2,†]*

[1] Daido Metal Co., Ltd., The European Headquarters, Winterhay lane, Ilminster, TA19 9PH, UK

[2] The Functional Materials Applied Research Group, Faculty of Health and Life Sciences, Coventry University, Coventry University, Priory Street, Coventry CV1 5FB, UK

ABSTRACT: Thin Ni composite coatings with hBN and WS_2 particles were ultrasonically-electrodeposited on Cu with no need of a surfactant. Although the combination of mechanical agitation and ultrasound yielded the best dispersions, ultrasound on its own during plating yielded coatings with a more uniform distribution of particles. Ni/hBN and Ni/WS_2 composite coatings electrodeposited under ultrasound were characterized by different methods: GD-OES to estimate particle content, XRD to analyse the preferred orientation, FIB-SEM to analyse the surface morphology and microstructure, and microhardness tests to measure the hardness. Whereas Ni/hBN composite coatings showed little difference compared to pure Ni deposits, the incorporation of WS_2 into Ni had a significant effect on the preferred orientation, the surface morphology and the grain size of the coatings, refining the Ni crystal down to the nano-scale. The latter had a significant effect in the hardness of the coatings, despite the 'soft' nature of the WS_2 particles.

KEYWORDS: Nickel; Composite coatings; Electrodeposition; Ultrasound

1. INTRODUCTION

The electrodeposition of Ni-based composites has received a wide attention in recent years due to the improved characteristics that these coatings may present [1]. Many of the studies available in the literature have been focused on the electrodeposition of composites with embedded 'hard' particles from Watts and sulphamate baths [2-5]. However, the incorporation of soft particles has received far less attention from the research community [6,7], despite of the improvement in the tribological performance that could be expected when soft particles are incorporated into Ni coatings due the high lubricity inherent to these particles. This high lubricity would be caused by the characteristic layered structure that these particles have: whereas atoms on same layer are closely packed and strongly bonded to each other, layers are relatively far apart and weakly bonded to each other [8].

[*] Corresponding autor: Dr. Ignacio Tudela
Tel: +44 7521160565, Email: ignacio.tudela@daidometal.com
[†] Corresponding author: Dr. Andrew J. Cobley
Tel: +44 7706955901, Email: aa2266@coventry.ac.uk

The electrodeposition of Ni composite coatings such as those reported in the studies previously referenced strongly relies on the addition of surfactants to the plating bath in order to achieve a good dispersion and prevent particle agglomeration in both the electrolyte and the coating. Nevertheless, the use of surfactants may affect process-control, waste effluent treatment, long-time stability and life-span of the electrolytes in Industry. For these reasons, other options are being evaluated for the electrodeposition of Ni-based composites with embedded particles, including the use of ultrasound in electrodeposition processes.

The use of ultrasound has already been proved successful in the electrodeposition of Ni composite coatings with embedded particles, not just in terms of improving the dispersion of particles in electroplating baths, but also to enhance the incorporation of well-disperse particles into the coating [9]. Hard particles such as Al_2O_3 [10], SiC [11] and TiN [12] have been successfully incorporated into Ni coatings electrodeposited from additive-free Watts formulations with the aid of ultrasound, generally resulting in Ni composite coatings with higher incorporation and more uniform distribution of particles. Regarding the use of ultrasound on the electrodeposition of Ni composite coatings with soft particles, very little research has been done so far. However, the work of García-Lecina et al. [13] on the electrodeposition of Ni composite coatings with inorganic fullerene-like WS_2 (IF-WS_2) nanoparticles is the best example of how ultrasound can significantly improve particle content, coating compactness and uniformity, resulting in better mechanical properties and enhanced tribological performance. In this latter case though, the addition of a surfactant (cetyl-trimethyl-ammonium bromide, CTAB) to the Watts bath formulated by the authors was still necessary to produce the Ni/IF-WS_2 composite coatings.

In this study the main goal was to produce thin Ni composite coatings with embedded WS_2 and hBN particles from an additive-free Watts bath. In this sense, the main objectives were: (i) to better understand how different agitation conditions may influence the dispersion of particles and their incorporation into electrodeposited Ni coatings from an additive-free Watts bath, (ii) to produce Ni composite coatings with WS_2 and hBN particles uniformly distributed within the Ni matrix, and (iii) to evaluate the characteristics of the novel Ni composites coatings that exhibited the best deposit quality. For this purpose, this study was structured in three main parts:

1. A first stage where WS_2 and hBN particles were dispersed in the Watts bath under different dispersing conditions: (i) ultrasound on its own, (ii) mechanical agitation on its own, and (iii) combined ultrasound/mechanical agitation.
2. A second stage focused on the production and qualitative evaluation of Ni/WS_2 and Ni/hBN composite coatings electrodeposited under different conditions: (i) ultrasound on its own, (ii) mechanical agitation on its own, and (iii) combined ultrasound/mechanical agitation.
3. A third stage focused on the detailed characterization of those Ni/WS_2 and Ni/hBN composite coatings produced during the second stage of the study that qualitatively presented a more uniform distribution of particles, higher particle content and less large agglomerates in the cross-section.

2. MATERIALS AND METHODS

2.1 EXPERIMENTAL SET-UP

The same Watts bath employed in a previous study focused on the electrodeposition of Ni deposits under ultrasound [14] was used in this study (Table 1). This Watts bath is currently used in industry for the manufacture of thin Ni coatings, and the electrodeposition from this bath is a kinetics-controlled process with a cathode current efficiency higher than 90% when operated at a current density of 4 A/dm^2. WS_2 and hBN particles (Figure 1) supplied by M K Impex Corp were employed in this study due to their lubricious nature, their commercial availability and their cost for a future scaling-up of the process. The concentration of particles in the Watts bath was always 15 g/L.

All the dispersion and electrodeposition experiments were conducted in the same set-up (Figure 2) used in the electrodeposition of Ni deposits under ultrasound [14] where a 600 mL beaker containing 500 mL of the Watts bath containing either WS_2 or hBN particles was immersed in an QS12 ultrasonic bath (Ultrawave Ltd). The QS12 ultrasonic bath, which was equipped with a built-in thermostat enabling the control of temperature up to 70 °C, operated at a frequency of around 32-38 kHz with an ultrasonic power of 0.180 W/cm^3 estimated by the calorimetric method [15-17]. In those experiments where mechanical agitation was required, a CAT R18 85W overhead stirrer (110 to 2000 rpm) equipped with a 3-point propeller shaft (50 mm wide) was used. An IPS2010 power supply unit (ISO-TECH) was used as the rectifier in all the electrodeposition experiments.

In relation to the ultrasonic conditions chosen, the effect of ultrasonic frequency and power indeed have a strong influence on the dispersion of particles in the bath and their incorporation into the Ni coatings during the electrodeposition, as discussed in a previous review paper by the authors [9]. Related to the ultrasonic frequency, although both mechanical and chemical effects of the introduction of ultrasound and the presence of acoustic cavitation in a liquid are observed at both low and high frequencies, mechanical effects (e.g. acoustic streaming, micro-jetting, release of shockwaves) are predominant at lower frequencies, whereas chemical effects (e.g. radical formation, sonoluminescence) are more significant at higher frequencies. These mechanical effects are the ones of special interest in composite electroplating due to (i) its ability to de-agglomerate large agglomerates and aggregates that otherwise would form and grow in the electrolyte and (ii) incorporate particles into the coatings [18,19]. In terms of power, the highest the power, the more effect ultrasound would have. Nevertheless, very high powers such as those achieved with an ultrasonic horn could have a detrimental effect on the incorporation of particles. In previous studies carried out by other researchers, an ultrasonic horn system was used to set the ultrasonic field during the electrodeposition of Ni [13] and Co [20] composite coatings containing IF-WS_2 particles. In this present study though, an ultrasonic bath set-up was chosen mainly due to the next reasons [9]:

1. Cavitation erosion. High-power ultrasonic horns, although very effective in order to disperse particles in short periods of time, produce very violent cavitation phenomena that may erode the surface of the deposits if they are placed near the transducer. Violent cavitation near the electrode can also have a negative effect in particle content in electrodeposited composite coatings, as particles may collide with the surface of the electrode under strong cavitation and then break away from there [13,21] or might be removed from the surface of the cathode by the 'scrubbing action' of cavitating bubbles.

2. Ultrasonic power. Extremely high acoustic pressures are achieved in a liquid when using a horn-type transducer in a small laboratory beaker. Nevertheless, these high ultrasonic powers are unlikely to be achieved in large plating tanks where the most feasible option would be the use of submersible units that consist of transducers with the same basic design as those used in ultrasonic baths.
3. Ultrasonic attenuation. Very high ultrasonic pressures can be achieved with a horn, which would obviously result in violent cavitation phenomena in the fluid. Nevertheless, most of the cavitation actually occurs near the emitter surface of the horn, as the highest pressures are achieved in this region. The formation of these cavitating bubbles has a negative effect when considering the application of ultrasound in bearing plating: a strong attenuation of the ultrasonic field in the region near the emitter surface due to the presence of the bubbles themselves [22,23]. This effect is much less significant in an ultrasonic bath, where a more homogeneous ultrasonic field can be set, resulting in the observation of cavitation phenomena not only near the emitter surface of the transducers, but also further away from this point.

2.2. Effect of ultrasound on the dispersion of particles in the Watts bath

2.2.1. Visual appearance of dispersions

WS_2 and hBN particles were dispersed for 30 minutes under different conditions: (i) mechanical agitation at 300 rpm in absence of ultrasound, (ii) ultrasound at 0.180 W/cm^3, and (iii) combined ultrasound/mechanical agitation at 0.180 W/cm^3 – 300 rpm. The resulting Watts/WS_2 and Watts/hBN dispersions were then observed by the naked eye in order to check the change in visual appearance with time once the dispersing method was stopped.

2.2.2. Particle size distribution experiments

Watts/WS_2 and Watts/hBN dispersions were also analysed by laser diffraction methods to estimate the particle size distribution in the dispersions. Such methods are based on the measurement of the intensity of light scattered as a laser beam passes through a dispersed particulate sample by different detectors. This data is then analysed by a proprietary algorithm, mainly based on the Mie theory [24], in order to estimate the size of the particles that created the scattering pattern. The laser diffraction system in the present study was a Mastersizer 2000 system (Malvern Instruments Ltd) which allowed the detection of particles with sizes ranging from 0.02 to 2000 μm.

The laser-diffraction methods for the analysis of the particle size distribution in liquid dispersions required the use of clear solutions with low particle content. Therefore, 500 mL dispersions consisting of very diluted Watts electrolyte (1 to 100 dilution) with a low concentration of WS_2 and hBN particles (0.1 g/L) were prepared by applying the three different dispersing methods previously defined for 30 minutes. Once the dispersion process was completed, particle size distribution measurements were carried out by circulating the dispersions through the Mastersizer 2000 system under 1000 rpm agitation for 30 seconds to ensure a proper circulation of the diluted Watts/WS_2 and Watts/hBN dispersions through the laser-diffraction system.

2.3. Electrodeposition of Ni composite coatings under different conditions

Ni/WS_2 and Ni/hBN composite coatings were electrodeposited under three different conditions: (i) mechanical agitation at 300 rpm in absence of ultrasound, (ii) ultrasound at 0.180 W/cm^3

and (iii) combined ultrasound/mechanical agitation at 0.180 W/cm^3 – 300 rpm. The same electroplating parameters previously defined for the electrodeposition of Ni coatings under ultrasound [14] were utilised in the present study (current density: 4 A/dm^2, plating time: 14 minutes). In all cases, the particles were first dispersed in the Watts bath for 30 minutes under the combined ultrasound/mechanical agitation dispersing method, since this approach apparently yielded the best Watts/WS_2 and Watts/hBN dispersions.

2.4. Characterization of Ni composite coatings electrodeposited under ultrasound

Different analytical methods were used to characterise the Ni-based composite coatings electrodeposited under ultrasound that exhibited the most promising features in terms of thickness uniformity, homogeneous particle distribution and reasonable particle incorporation. Glow Discharge – Optical Emission Spectroscopy (GD-OES) analysis of the central area of the deposits was carried out with a SPECTRUMA GDA 750 spectrometer equipped with a Grimm-type glow discharge source of 2.5 mm in diameter in order to analyse the particle content in the composite coatings. X-Ray Diffraction (XRD) analysis was carried out with a Bruker D8 ADVANCE equipment to evaluate the effect that the incorporation of particles into the Ni coatings had on the crystal orientation of the deposit. The surface morphology and crystal structure of the coatings was analysed with a FEI Nova 600 Nanolab Dualbeam Focused Ion Beam-Scanning Electron Microscope (FIB-SEM) system. GD-OES, XRD and FIB-SEM analyses were always performed in the central area of the samples. Microhardness tests were performed on the cross-section of the deposits with a MicroWiZhard HM 221 system from Mitutoyo to evaluate how the incorporation of particles into the coating and their effect on its grain structure affected the hardness of the electrodeposited Ni composite coatings. For this purpose, samples were horizontally cut near the horizontal symmetry axis of the deposit, mounted in epoxy resin and thoroughly polished. A load of 2 g-force was applied for 10 seconds to measure the hardness in five random locations around the central area of the cross-section to avoid any effect of the Cu substrate on the hardness measurements.

3. Results and Discussions

3.1. Effect of agitation method on the dispersion of particles in the Watts bath

3.1.1. Watts/WS_2 dispersions

Figure 3 shows the visual appearance of the Watts/WS_2 dispersions that were prepared under the three different dispersing conditions studied: ultrasound at 0.180 W/cm^3, mechanical agitation at 300 rpm, and combined ultrasound/mechanical agitation at 0.180 W/cm^3 – 300 rpm. No visual difference was observed in the dispersions produced under different conditions immediately after the end of the process, as a dense, black solution was obtained in all cases. After 60 minutes, a clear green colour was apparent in the solution produced under mechanical agitation at 300 rpm, whereas the solutions produced with ultrasound on its own and the combined process exhibited a much darker green colour. This indicated that the 'sinking rate' of the particles dispersed under mechanical agitation at 300 rpm (no ultrasound was applied) was higher than for the particles dispersed with the other methods where ultrasound was employed. After 240 minutes, the dispersions produced with either ultrasound or combined agitation became slightly clearer, meaning that particles in both solutions were also progressively sinking

after agitation had ceased. Nevertheless, the solution produced with mechanical agitation presented a much clearer green colour, and the formation of a black sludge at the bottom of the beaker was clearly noticed. This confirmed that the dispersion of WS_2 particles in the plating solution obtained with mechanical agitation was not as good as those dispersions achieved where ultrasonic dispersion was utilised.

Particle size distribution experiments were performed on diluted Watts/WS_2 dispersions to observe the effect that the different dispersing methods had on the particle size distribution (Figure 4). The combined ultrasound/mechanical agitation at 0.180 W/cm^3 – 300 rpm was the best dispersing method out of the three studies in this work, followed by the 'ultrasound only' method at 0.180 W/cm^3, which yielded slightly higher results, whereas the dispersions with the worst quality in terms of particle size were achieved with the 'mechanical agitation only' method at 300 rpm. In all cases, single modal Gaussian-alike distribution curves were obtained.

The results obtained during the particle size distribution experiments of the diluted Watts bath/WS_2 dispersions agree to some extent with the visual appearance of the 'real' electrolytes containing the 'real' concentration of particles. They suggest that the best way of dispersing WS_2 particles was to combine mechanical agitation with ultrasound, closely followed by the use of ultrasound on its own, whereas the use of mechanical agitation on its own was clearly the worst dispersing method in both visual appearance and particle size distribution experiments.

3.1.2. WATTS/HBN DISPERSIONS

Figure 5 displays the visual appearance of the Watts/hBN dispersions that were prepared under the three different dispersing conditions studied. The best Watts/hBN dispersion was achieved by combining ultrasound and mechanical agitation, as a homogeneous, white-green solution with no signs of large aggregates was produced under these conditions. The worst dispersion was obtained when mechanical agitation was used in the absence of ultrasound, as it was quite non-homogeneous with the presence of large agglomerates. In this later case, particles started to sink immediately after the end of the dispersion process. However, after 30 minutes, the bulk solution in all of the Watts/hBN dispersions appeared quite similar, as they presented a turbid green colour. This was due to the hBN particles agglomerating and sinking, resulting in the formation of a white sludge at the bottom of the beaker. Nevertheless, the sludge was more compact and difficult to re-disperse in the hBN dispersion produced under mechanical agitation.

As with the Watts/WS_2 dispersions, particle size distributions experiments were also conducted on diluted Watts/hBN dispersions prepared under different conditions (Figure 6). Again, the dispersions prepared under mechanical agitation at 300 rpm in the absence of ultrasound showed the lowest quality in terms of particle size distribution, whereas both dispersing methods where ultrasound was used yielded very similar results. The difference between the presence or absence of ultrasound in the dispersion was also reflected in the single-modal Gaussian-like distribution curves obtained for the dispersions prepared with the combined and 'ultrasound only' methods, as opposed to the 'mechanical only' method, where a bi-modal curve was obtained. This bi-modal curve, where the largest peak indicates the presence of large agglomerates with particle sizes in the order of 100 μm roughly agree with the results obtained in the visual appearance experiments conducted on the dispersions prepared with the 'mechanical only' method, where particles started to form very large agglomerates that could be clearly seen by the naked eye.

As in the case of the Watts/WS_2 dispersions, the particle size distribution experiments of the diluted Watts/hBN dispersions also agree to some extent with the visual appearance of the 'real' Watts electrolyte containing the 'real' concentration of hBN particles, pointing again to the combined ultrasound/mechanical agitation as the best conditions out of the three studied in this work to disperse hBN particles in the Ni Watts bath.

3.1.3. DISCUSSION OF THE EFFECT OF AGITATION METHOD ON THE DISPERSION OF PARTICLES IN THE WATTS BATH

For both WS_2 and hBN particles the best Watts/particle dispersions were obtained when combining ultrasound and mechanical agitation, whereas the worst dispersions were achieved when using mechanical agitation on its own. In this sense, the visual appearance of the 'real' Watts/hBN dispersions clearly indicate why the combination of ultrasound and mechanical agitation works better than using either ultrasound or mechanical agitation on its own: (i) from the 'macrodispersion' point of view, mechanical agitation contributed to achieve a more homogeneous dispersion, preventing the larger agglomerated particles from sinking to the bottom of the beaker, and (ii) from the 'microdispersion' point of view, the presence of ultrasound enhanced the de-agglomeration of agglomerated particles due to the formation of cavitating bubbles and the physical effects inherently related to their presence [25]: (a) micro-turbulence due to the oscillation of the acoustic pressure and cavitation fields, and (b) high speed particle collisions induced by mechanical effects of acoustic cavitation (i.e. acoustic streaming, microjetting, shockwaves) which may brake van der Waals forces within particle agglomerates.

It is interesting to note that, whereas a significant difference in terms of dispersion homogeneity was observed in the 'real' Watts/hBN dispersions prepared with the combined method and ultrasound on its own, the particle size distribution experiments conducted on equivalent diluted dispersions, although did also suggest that the combined method was better than ultrasound on its own, did not reflect this difference. The opposite was observed in the Watts/WS_2 dispersions, where clear differences were observed in the particle size distribution experiments performed on diluted dispersions prepared with the combined method and ultrasound own its own, whereas no significant difference was observed in the 'real' Watts/WS_2 dispersions prepared with both methods. In this regard, although both approaches proved quite effective as a comparative tool to select the best of the dispersing methods studied here, the authors are aware that they also present some limitations. For the visual appearance experiments, the main drawback would be the relative subjectivity of the results, especially in the case of the Watts/WS_2 dispersions where the black colour of the solutions Ni Watts electrolyte containing WS_2 particles would make it quite difficult to distinguish the difference in terms of particle sinking and clarity of the suspension in the early moments after the dispersion. For the particle size distribution analysis, the main drawbacks were inherently related to the analytical technique employed, laser diffraction-based particle sizing, due to different aspects:

- An approximated refractive index (RI) was considered for the particles and the electrolyte (RI = 2.75 for the WS_2 particles based on the RI values of thin WS_2 films [26]; RI = 1.8 for the hBN particles [27] and RI = 1.33 for the diluted Ni Watts electrolyte). Therefore some inaccuracy in the measured particle size results is expected [28].
- The reason for using a diluted Ni Watts electrolyte containing a very low concentration of particles is due to the need to have clear solutions in order to have a proper transmission of the laser through the samples. This is required to ensure relatively low

laser obscuration once the solids are dispersed and is inherent to the use of laser diffraction-based particle sizing methods [29]. Although the pH was adjusted that of 'real' Ni Watts bath, the diluted nature of the dispersions means that changes in the particle size could occur due to the highly conductive nature of the Ni Watts bath and the higher concentration of the particles in the real solutions. Not many authors explain in detail in which conditions their experiments were carried out [30]. The degree of dilution of the electrolyte and the (low) concentration of particles should be clearly stated, especially if one considers that factors such as increasing ionic strength [31] and particle concentration [32] may further promote the agglomeration of the particles in the plating bath.

- The analytical method itself, which may not properly account for the 'non-spherical' nature of some particles, and the proprietary numerical algorithms used in the laser diffraction equipment, which are quite complex yet not fully-validated experimentally [33].

3.2. ELECTRODEPOSITION OF NI COMPOSITE COATINGS UNDER DIFFERENT AGITATION CONDITIONS

3.2.1. NI/WS_2 COMPOSITE COATINGS

Figure 7 A displays some examples of the Ni/WS_2 composite coatings electrodeposited on Cu substrates under different agitation conditions. Dull, dark grey deposits were obtained when ultrasound was used on its own, while dull, light grey coatings were produced under combined ultrasound/mechanical agitation. In both cases, sludgy deposits of fine powder were observed in the upper edge of the samples, particularly under combined ultrasound/mechanical agitation. No acceptable Ni/WS_2 composite coatings were electrodeposited under mechanical agitation in absence of ultrasound, as particles agglomerated on the surface of the Cu substrate and blocked the active area of the cathode during plating. This layer of agglomerated WS_2 particles was hard to remove by rinsing with deionised water, although it would fall off the substrate quite easily once dried. Cross-sections of Ni/WS_2 composite coatings produced under ultrasound and combined ultrasound/mechanical agitation conditions were further examined as shown in Figure 7 B (cross-sections of the composite coatings produced under mechanical agitation were not further evaluated because the deposits came off the Cu substrate while cutting, mounting and polishing the samples for their evaluation with the optical microscope). Deposits with the expected thickness (around 5-7 μm) containing many WS_2 particles were produced under ultrasound on its own, whereas significantly thinner composite coatings (around 2-3 μm) with much lower WS_2 content were electrodeposited under combined ultrasound/mechanical agitation.

3.2.2. NI/HBN COMPOSITE COATINGS

Figures 8 A displays the surface finish of Ni/hBN composite coatings produced under ultrasound, mechanical agitation or combined ultrasound/mechanical agitation. A good surface finish was observed in all the deposits, and no apparent variation was noticed in the composite coatings electrodeposited under different plating conditions. The cross-section of the Ni/hBN composite coatings produced under different electroplating conditions is displayed in Figure 8 B. Coatings plated under mechanical agitation showed large agglomerates with a less homogeneous distribution of the hBN particles, whereas finer particles were clearly noticed in the composite coatings electrodeposited under ultrasonic and combined conditions.

Nevertheless, coatings plated under ultrasound on its own presented far more particles than the ones plated under combined ultrasound/mechanical agitation.

3.2.3. Discussion of the effect of the agitation conditions on the electrodeposition of Ni composite coatings

The results obtained for the Ni/WS_2 composite coatings in terms of surface finish, thickness and particle incorporation were electrodeposited under ultrasound on its own suggests that the way the ultrasonic field is set and how it may interact with the stirring of the electrolyte has a critical impact on the quality of the electrodeposited composite coatings. In this sense, mechanical agitation seemed to counteract the effect of ultrasound in terms of particle incorporation. This could be due to the nature of the fluid flow that occurs when agitating with the overhead stirrer. In this situation, the flow is parallel to the surface of the cathode and particles may be 'removed' from near the surface of the substrate reducing the concentration of the particles in the cathode-electrolyte interface, resulting in a lower incorporation of particles into the coating. The fact that only the smallest WS_2 particles were incorporated into the coatings prepared under the combined method would be in agreement with this consideration. Cavitating bubbles near the surface would also be affected by the action of the overhead stirrer, being less effective in those areas near the cathode surface and this would reduce their ability to de-agglomerate some of the large WS_2 particles, which in turn would partially block the surface of the substrate, leading to the thinner deposits obtained under ultrasound/mechanical agitation. This would also explain the sludgy areas observed around the upper edge of samples electrodeposited under ultrasound/mechanical agitation which were far more extended than in the deposits produced under ultrasound. For the Ni/WS_2 composite coatings electrodeposited under mechanical agitation in absence of ultrasound, the lack of 'de-agglomerating' action on the large WS_2 agglomerates near the surface would result in massive deposition of WS_2 on the surface of the cathode by electrophoretic forces, which would block the surface of the cathode and hence prevent the deposition of Ni.

These results are to some extent in agreement with those recently reported by García-Lecina et al. [13] on their Ni/IF-WS_2 composite coatings also electrodeposited from a Watts bath. In their case, the way to overcome all these issues was to add a surfactant, CTAB, to the Watts bath. In the present work, CTAB was not necessary to obtain acceptable Ni/WS_2 composite coatings under ultrasound due to two main reasons:

- The WS_2 particles used in this study were 1-2 orders of magnitude larger than their IF-WS_2 nanoparticles (particle size around 40-120 nm forming clusters with a size up to 600 nm). And as they commented in their paper, the '*smaller the agglomerated WS_2 particle groups, the higher the opportunity for attraction by the electric field*' [13].
- The nature of the ultrasonic field near the surface of the cathode. In the study here presented, electrodeposition under ultrasound in absence of mechanical agitation was critical in order to obtain Ni/WS_2 composite coatings with acceptable surface finish and thickness. The different ultrasonic set-up used in the present study (32-38 kHz ultrasonic bath) would also affect cavitation phenomena occurring near the surface of the cathode.

Regarding the Ni/hBN composite coatings, it again seemed that the stirring of the Ni bath with the overhead stirrer counteracted the effect of ultrasound in terms of particle incorporation, as previously described for the Ni/WS_2 composite coatings. In this case though, although the 'removal' of particles from the cathode-electrolyte interface due to the fluid flow developed near

the surface of the Cu substrate by the overhead stirrer would also occur, deposition and blocking of the cathode surface due to the agglomeration of the hBN particles did not take place. This is evidenced by the fact that all the Ni/hBN composite coatings presented the same thickness with no dependence on the agitation conditions used during the electrodeposition. This would be due to different physical-chemical properties of the surface of the particles such as the electrokinetic potential and charge of the particles, which result in the electrophoretic deposition of WS_2 particles, as previously mentioned. Such differences in the physical-chemical properties of the surface of the particles which would also explain why hBN particles took much shorter times to agglomerate and sink that the WS_2 particles in the visual appearance experiments of the Watts bath/particle dispersions.

On another hand, it was observed that, despite that very large agglomerates may form in the dispersions according to Figures 4 and 6, the size of the particles incorporated into the coatings, particularly in the case of the Ni/hBN composite coatings, was fairly small. The fact that the goal of this research was to produce thin composite coatings would indeed have an influence on this. Another reason for this would be what Ger [34] called the 'effective particle' in terms of particle size and incorporation. Related to this, whereas particles may aggregate quite seriously in some cases (see curves in Fig. 6 for the 'mechanical only' Watts/hBN dispersion), only the smaller and better-dispersed particles and agglomerates are incorporated into the coatings. As colloidal interactions would govern the codeposition of the particles [35], the existence of 'adhesion forces' counteracting the action of 'removal forces' that are more effective the particles are well-dispersed in the electrolyte [34], and hence why only the fraction of well-dispersed particles and smaller agglomerates or aggregates are usually incorporated into electrodeposited coatings [34,36], even when ultrasound is used to dispersed the particles [10]. In this sense, although particle agglomeration cannot be completely avoided once particles are added to a electroplating bath [34], ultrasound does improve the dispersion of particles and hence improve the number of the so-called 'effective particles', according to previous observations from other authors [10] and the results here presented.

3.3. CHARACTERIZATION OF NI-BASED COMPOSITE COATINGS ELECTRODEPOSITED UNDER ULTRASOUND

Ni/WS_2 and Ni/hBN composite coatings electrodeposited under ultrasound at 0.180 W/cm^3 were selected for further characterization as these plating conditions were the only ones which produced composite coatings with acceptable quality in terms of thickness uniformity, homogeneous particle distribution and reasonable particle incorporation.

3.3.1. PARTICLE CONTENT

Figure 9 displays data from GD-OES analysis performed on Ni/WS_2 and Ni/hBN composite coatings electrodeposited under ultrasound as a depth profile of the concentration of the different elements present in the sample expressed in percentage by weight. The graphs show that the Ni/WS_2 composite coatings presented higher particle content in terms of weight percentage (up to 1 order of magnitude in some areas) than the Ni/hBN composite coatings electrodeposited under the same conditions (Watts electrolyte, 15 g/L of particles in the bath, ultrasound at 0.180 W/cm^3, etc.). It must be noted though the difference in density of the different particles, which is 7500 kg/m^3 for the WS_2 particles and 2300 kg/m^3 for the hBN particles according to the supplier (M K Impex Corp). This actually implies that, when one takes into account the difference of density of the different particles, the difference in terms of particle

content between the Ni/WS_2 and the Ni/hBN composite coatings is not as high as it seems when only considering the particle content in weight percentage. In terms of the distribution of particles within the coating, the Ni/WS_2 composites presented three different areas: (i) a region near the surface of the coating with a high concentration of WS_2 particles near the surface, (ii) the bulk coating with a lower yet constant concentration of WS_2 particles, and (iii) a region near the coating-substrate interface where the particle content doubles that of the bulk coating. The GD-OES depth profiles obtained for the Ni/hBN composites point to a slightly different trend: (i) a region near the surface of the coating with high hBN particle content, and (ii) the bulk coating with low particle content which progressively increases towards the coating-substrate interface, where it reaches its highest value. The high particle content observed in the region near the surface in both composites can be attributed to the adherence of some of the particles in the electrolyte to the surface of the coating once the electrodeposition process is completed, a phenomenon quite common when depositing composite coatings with embedded particles, as noticed in other works where GD-OES was used to analyse the depth profile of different composite coatings [37-39].

The differences observed between the Ni/WS_2 and Ni/hBN composite coatings in terms of particle content and distribution within the coating would again be related to the different physical-chemical properties of the surface of the particles (electrokinetic potential, charge, etc.). WS_2 particles would in this sense be more attracted to the surface of the cathode than the hBN particles under the same electrodeposition conditions, resulting in a apparently higher incorporation of particles into the coating immediately after the electrodeposition starts, followed by a constant ´replenishment´ of WS_2 from the bulk solution to the cathode-electrolyte interface, and hence a constant content of WS_2 particles in the bulk coating. Such conditions would not be achieved in the case of the hBN particles, as these particles would not be as 'attracted' to the cathode surface as the WS_2 particles, and hence the progressive decrease of particle content from the coating-substrate interface towards the bulk coating. In other words, if the attraction/incorporation of particles was treated as a 'traditional' electrochemical reaction, the incorporation of WS_2 particles would be considered as a kinetic/mixed-controlled process, whereas the incorporation of hBN particles would be considered as a mass transport-controlled process.

From these GD-OES results, the estimated average particle content in the Ni/WS_2 and Ni/hBN composite coatings was around 1.0 % by weight of WS_2 particles and 0.2 % by weight of hBN particles, respectively. These values were estimated considering W and B content in the Ni/WS_2 and Ni/hBN composite coatings, respectively. The reasons for this were:

- Relatively higher S reading near the surface in the Ni/WS_2 composite coating due to presence of sulphate from Watts bath (molar relation between S and W was always 2 except in the superficial region, where it progressively increases towards the surface of the coating).
- Relatively higher N reading near the surface in the Ni/hBN composite coating due to N_2 from air (molar relation between N and B was always 1 except in the superficial region, where it slightly increased towards the surface of the coating).

3.3.2. CRYSTAL ORIENTATION

Figure 10 displays the XRD scans conducted for both composite coatings. While the Ni/hBN presented high peaks for (111) and (200) crystal planes in a similar way to those previously observed in 2θ spectra of Ni deposits electrodeposited under different ultrasonic conditions

[14], the Ni/WS_2 deposits showed a significant decrease in the intensity of the (200) planes when compared to height of the peak observed for the (111) planes. In addition, a relative increase was observed for the (220), (311) and (222) crystal planes when compared with the intensity of the (111) planes for the Ni/WS_2 composites coatings. For the latter, the 2θ scans also showed the presence of the WS_2 particles embedded in the Ni matrix, as (006) and (008) crystal planes associated to the presence of WS_2 were quite noticeable.

The 'Relative Texture Coefficient' (RTC) method [40] was used in order to quantify the different crystal planes observed in the 2θ scans of the different Ni-based composite coatings evaluated in this study. This method, which is extensively used for in electrodeposited metal-based coatings [39,41-44], yields normalized and quantitative data of the different crystals planes observed in a sample and eliminates the roughness effect of the deposits analysed. RTC for a certain (hkl) crystal plane is defined as:

$$\mathrm{RTC}_{(hkl)} = 100 \times \frac{\mathrm{I}_{(hkl)}/\mathrm{I}_{(hkl),\mathrm{P}}}{\sum_1^5 \mathrm{I}_{(hkl)}/\mathrm{I}_{(hkl),\mathrm{P}}} \quad (1)$$

where $\mathrm{I}_{(hkl)}$ is the intensity of the reflection for the (hkl) crystal plane in the analysed coating and $\mathrm{I}_{(hkl).\mathrm{P}}$ is the intensity of the reflection for said crystal plane in a standard Ni powder sample with random orientation. The denominator in Equation (1) is the sum the relation between $\mathrm{I}_{(hkl)}$ and $\mathrm{I}_{(hkl).\mathrm{P}}$ for all the different Ni crystal planes observed in the 2θ spectrum, which for the case of Ni are (111) for $2\theta \approx 44.50º$, (200) for $2\theta \approx 51.85º$, (220) for $2\theta \approx 76.38º$, (311) for $2\theta \approx 92.94º$ and (222) for $2\theta \approx 98.45º$ [45].The intensities for the crystal planes in the standard Ni powder sample with random orientation are $\mathrm{I}_{(111).\mathrm{P}} = 999$, $\mathrm{I}_{(200).\mathrm{P}} = 420$, $\mathrm{I}_{(220).\mathrm{P}} = 161$, $\mathrm{I}_{(311).\mathrm{P}} = 144$ and $\mathrm{I}_{(222).\mathrm{P}} = 39$ [45].

$\mathrm{RTC}_{(hkl)}$ values were estimated for the Ni/WS_2 and Ni/hBN composites electrodeposited under ultrasound at 0.180 W/cm³ (Figure 11 A). For the Ni/hBN composite, a small decrease in $\mathrm{RTC}_{(200)}$ and $\mathrm{RTC}_{(222)}$ was noticed compared to those of Ni deposits produced under ultrasound at the same ultrasonic power, along with a more significant increase in $\mathrm{RTC}_{(111)}$ (almost a 100% increase compared to that of Ni coatings electrodeposited under ultrasound at the same power [14]). However, $\mathrm{RTC}_{(hkl)}$ values were completely different for the Ni/WS_2 composites, where $\mathrm{RTC}_{(222)}$ > 40% while the other $\mathrm{RTC}_{(hkl)}$ remained below 20%, with $\mathrm{RTC}_{(200)}$ presenting the lowest value, as opposed to what was observed for the Ni/hBN composite and Ni deposits [14] where $\mathrm{RTC}_{(200)}$ always presented the highest values. The very large $\mathrm{RTC}_{(222)}$ value estimated for the Ni/WS_2 composite is due to the own nature of the RTC method: as the intensity of the reflection for a (hkl) crystal plane in the analysed deposit, $\mathrm{I}_{(hkl)}$, is divided by the intensity of the reflection of that same crystal in the randomly oriented powder, $\mathrm{I}_{(hkl).\mathrm{P}}$, in those cases where $\mathrm{I}_{(hkl).\mathrm{P}}$ may be very small, as in the case of (220), (311) and (222) crystal planes, $\mathrm{RTC}_{(hkl)}$ will be relatively higher.

Electrocrystallization on [100] and [110] directions is straightforwardly associated with (200) and (220) crystal planes [43], respectively. On the other hand, [111] and [311] orientations can be related to a dispersed [211] orientation [46-48], which means that (111), (311) and (222) crystal planes may be related to the presence of Ni crystals with a [211] orientation. Therefore, $\mathrm{RTC}_{[hkl]}$ values were also estimated by defining $\mathrm{RTC}_{[100]} = \mathrm{RTC}_{(200)}$, $\mathrm{RTC}_{[110]} = \mathrm{RTC}_{(220)}$ and $\mathrm{RTC}_{[211]} = \mathrm{RTC}_{(111)} + \mathrm{RTC}_{(311)} + \mathrm{RTC}_{(222)}$ (Figure 11 B). A small decrease in $\mathrm{RTC}_{[100]}$ and small increase in $\mathrm{RTC}_{[211]}$ was observed for the Ni/hBN composite compared with the $\mathrm{RTC}_{[hkl]}$ observed for the Ni

deposits produced under ultrasound at 0.180 W/cm^3. The increase in $RTC_{[211]}$ and decrease in $RTC_{[100]}$ were far more significant for the Ni/WS_2 composite, which clearly showed a strong [211] preferred orientation ($RTC_{[211]}$ > 70%). A significant increase in the presence of crystals with a [110] orientation was also noticed for this composite ($RTC_{[110]}$ > 15%).

The crystal orientation in electrodeposited Ni coatings is believed to be under the influence of the so-called 'inhibition effect' [49 - 52]. In this sense, whereas 'inhibition-free' Ni electrocrystallizes with a [100] orientation, Ni growing with a [110] orientation is the result of electrocrystallization being inhibited by adsorbed atomic hydrogen (H_{ads}) covering the surface of the cathode. In addition, the electrocrystallization of Ni in the [210] orientation is promoted by the presence of gaseous hydrogen (H_2) caused by massive hydrogen evolution at the cathode, while the electrocrystallization of Ni on the [211] direction is the least inhibited by the presence of colloidal/precipitated $Ni(OH)_2$ near the electrolyte-cathode interface.

In previous studies, an increase in $RTC_{[100]}$ and decrease in $RTC_{[211]}$ coefficients were observed for electrodeposited Ni coatings under ultrasound at high powers compared to Ni deposits produced under mechanical agitation and silent/still conditions [14], suggesting that less inhibiting species were present in the cathode-electrolyte interface. However, this situation changed when either WS_2 or hBN particles were added to the Ni Watts bath and composite coatings were produced under the same ultrasonic conditions, especially in the case of the Ni/WS_2 coatings, for which $RTC_{[211]} \approx 7 \times RTC_{[100]}$. The results observed for the Ni/hBN and Ni/WS_2 composite coatings agree with previous observations made by Pompei et al. [7] and García-Lecina et al. [13], respectively, as in both previous studies the incorporation of either hBN or IF-WS_2 particles resulted in an increase in the relative intensity of XRD peaks associated to a [211] growth direction compare to the peak related to the [100] orientation. Such higher presence of Ni crystals growing in the [211] direction indicates an increase in precipitated and/or colloidal $Ni(OH)_2$ in the cathode-electrolyte interface due to the alkalization of the interface by either an increase in the hydrogen evolution on the surface of the cathode or the adsorption of atomic hydrogen. Hydrogen evolution on the surface of the cathode was not noticed when preparing both Ni/hBN and Ni/WS_2 composite coatings under ultrasound, meaning that the most probable option for the increase of the proportion of [211] textures in both coatings was the adsorption of atomic hydrogen.

Considering that the Ni/WS_2 composite coatings presented a higher particle content by weight, and that these coatings also presented a more significant change in the crystal orientation than the Ni/hBN composite coatings, the results not only suggest that the WS_2 particles have a greater effect than the hBN particles on the orientation of the crystals due to either higher incorporation or different physical and chemical properties of the particles, but also that the atomic hydrogen was adsorbed on the surface of the particles rather than on the surface of the cathode. In this sense, Pavlatou and Spyrellis [42] suggested that the presence of particles had an effect on the orientation of the crystals by affecting the composition in the cathode-electrolyte interface due to the adsorption of atomic hydrogen in the surface of the particles. This adsorption results in a local alkalization of the cathode-electrolyte interface, leading to the crystallization of Ni crystals with a [211] preferred orientation. A similar increase in the proportion of crystals with a [211] preferred orientation has also been observed by other authors for different particles dispersed in a Ni Watts bath. McNormack et al. [53] noticed that, the higher the concentration of Y_2O_3, the more significant was the change of growth mode from [100] to [211] of the Ni coatings they were producing. Similar results have been previously

obtained by other authors for Ni/SiC [54-56] and Ni/Al_2O_3 [57] composite coatings from different electrolytes.

3.3.3. SURFACE MORPHOLOGY AND COATING STRUCTURE

Tilted FIB-SEM images of Ni/WS_2 and Ni/hBN composite coatings electrodeposited under ultrasound at 0.180 W/cm^3 are displayed in Figure 12. Nodule-shaped structures similar to those previously observed in Ni deposits produced in prior studies [14] were noticed in some areas of the surface of the Ni/hBN composite coatings. However, a completely different surface morphology with no signs of either nodular structures or grooves was observed for the Ni/WS_2 coatings.

High-magnification FIB-SEM images of Ni/WS_2 and Ni/hBN composite coatings are also displayed in Figure 13. As previously pointed out, the surface structure of the Ni/WS_2 composite coatings differed significantly from the surface structure observed in Ni deposits produced in prior studies [14]. No surface morphologies resembling Ni grains with [100], [110] or [211] orientations such as those reported for crystals with said orientations reported by other authors [43,44,48,58] were noticed. Instead, a random distribution of spherical and irregular structures was observed suggesting that WS_2 particles near the surface of the coating were covered by thin Ni layers as in the Ni/Mo composite coatings observed by Kubistzal et al. [59]. A similar structure was also noticed by Mohajeri et al. [60] for their Ni/WC coatings. In the latter, the authors suggested that the particles and the metal were deposited on the surface of the cathode, and Ni gradually grew on the particles to cover the gap between the grains. Nevertheless, despite the similarities of the morphology of both Ni/WS_2 and Ni/Mo composites, the sphere-like structures of the deposits containing WS_2 particles were about one order of magnitude smaller. In addition, Ni/WS_2 composite coatings were more compact, as the Ni/Mo deposits presented deep narrow pores and the Ni/WC coatings also had significant gaps and holes over the surface. For the Ni/hBN composite coatings deposited under ultrasound, although it was harder to associate the structure of the Ni crystals to the different orientations they may have, some Ni grains with a surface morphology similar to that Ni grains with a [100] orientation reported elsewhere [43,44,48,58] were relatively easy to find over the surface, although not as obvious as in the electrodeposited Ni coating previously studied [14].

The cross-section of the Ni/WS_2 and Ni/hBN composite coating electrodeposited under ultrasound at 0.180 W/cm^3 was further analysed by FIB-SEM to observe any possible effect of the incorporation of particles into the coatings (Figure 14). An apparently nano-crystalline structure of Ni with many WS_2 particles intercalated in the metal matrix was observed for the Ni/WS_2 composite coatings instead of the columnar structure observed in Ni deposits produced in absence of ultrasound and the more fragmented structure of Ni deposits produced under ultrasound [14]. hBN particles seemed to have no significant effect on the grain size and the microstructure of the deposit, as Ni columnar crystals were still visible in the Ni/hBN composite coatings. These composite coatings presented in fact a similar structure to that observed in Ni deposits produced under ultrasound, although the structure of the composite coating seemed slightly less fragmented than that of the pure Ni deposit.

The grain-refinement effect of particles in electroplated coatings, which generally results in finer surface morphology and smoother finish, has been extensively reported in the past, not only when the electrodeposition is carried out in silent conditions [1,61], but also in the presence of ultrasound [12,13,62]. However, the evidence for this grain-refinement effect of particles has often relied on either SEM images of the surface or XRD data (e.g. Scherrer

equation [63]). Lampke et al. [64] did show the effect that both ultrasound and the addition of TiO_2 nanoparticles to the plating solution had on the grain size and structure by Electron Back-Scatter Diffraction (EBSD) analysis, although in their case the modification of the crystal structure was not as significant as the grain refinement achieved for the Ni/WS_2 composite coatings shown in Figure 14. The crystal structure of the Ni/WS_2 composite coatings here reported constitutes, to the best knowledge of the authors, the most significant proof ever reported of the grain refinement effect achieved by the incorporation of particles into electrodeposited Ni coatings.

3.3.4. HARDNESS

Microhardness tests were performed on the Ni/hBN and Ni/WS_2 composite coatings produced under ultrasound at 0.180 W/cm^3 to have an initial idea of the effects of the incorporation of the particles and the modification in the microstructure of the composite coatings on the mechanical properties of the electrodeposited Ni coatings. Compared to pure Ni deposits electrodeposited under silent conditions and ultrasound at the same power [14], the Ni/WS_2 composite coatings showed significantly enhanced hardness, whereas lower hardness values were obtained for the Ni/hBN composite coatings.

Grain size is one of the main controlling factors in the hardness of electroplated coatings [65], and many different studies have related grain refinement and increase in hardness of electrodeposited Ni coatings [66]. Therefore, it should not be a surprise that the incorporation of WS_2 particles into the Ni coatings resulted in an increase in hardness of around 16% compared to the values observed for pure Ni deposits plated under ultrasound at the same ultrasonic power (0.180 W/cm^3) and around 27% higher than what was observed for pure Ni deposits plated under silent conditions. Nevertheless, it seemed a relatively small increase compared to what should be expected of a Ni matrix with an apparent nano-crystalline structure. Other authors have reported a greater increase in the hardness of Ni coatings with embedded particles. For example, Xue et al. [67] observed an increase from ≈260 HV for pure Ni deposits to ≈620 HV for Ni/CeO_2 coatings produced under ultrasound, while García-Lecina et al. [55] noted an increase from ≈250 HV for pure Ni deposits to ≈460 HV for Ni/Al_2O_3 composites, also plated under ultrasound. An even greater increase in hardness for Ni/Al_2O_3 coatings was observed by Feng et al. [68] for deposits produced in a solution where Al_2O_3 particles were dispersed with ultrasound prior to the electrodeposition (from ≈280 HV for pure Ni to ≈580 HV for Ni/Al_2O_3 coatings). The enhancement in hardness reported in the present work for the Ni/WS_2 deposits is however comparable to the results obtained by other authors for Ni deposits containing SiC [69] and TiO_2 particles [70,71].

It must be noted that, in the study here presented, inherently soft, lubricant WS_2 particles (WS_2 Mohs hardness is 1-1.5 vs. 4 of Ni) were used instead of the hard particles used elsewhere, and this might have a counter-effect on the hardness of the deposit. Related to this, Sivandipoor and Ashrafizadeh [72] noticed a 60 % decrease in hardness in their electroless plated Ni-P coatings when WS_2 particles were incorporated into the deposit, Balaji et al. [73] observed a progressive reduction in hardness when increasing the proportion of PTFE particles in electrodeposited bronze, and Stanovic and Gojo [74] reported that, while the addition of hard particles such as Al_2O_3, SiC and B_4C increased the hardness of electrodeposited Cu, the incorporation of soft particles such as MoS_2, $BaSO_4$ and graphite lead to a reduction in the hardness of the coatings compared to pure Cu deposits. Therefore, it can be concluded that the main cause for the hardness increase observed in the Ni/WS_2 composites is the significant grain refinement

achieved. The 'softening' effect brought about by the addition of soft lubricant particles is quite evident in the Ni/hBN composite coatings (hBN Mohs hardness is 1-2 vs. 4 of Ni). For these coatings, despite the modification of the structure of the deposits in terms of a more fragmented structure with less and thinner Ni columnar crystals and more refined grains, the presence of soft hBN particles led to a reduction in the microhardness of around 6% compared to pure Ni coatings plated under silent/still conditions. Pompei et al. [7] reported different data that may contradict the results presented here, as they obtained Ni/hBN composite coatings with hardness values of around 500 HV. Nevertheless, they used a commercial surfactant to refine the grain size, already obtaining an increase in hardness from 280 HV to 400 HV before incorporating the particles into their coatings.

4. CONCLUSIONS

The present study demonstrates how ultrasound can improve the electrodeposition of Ni-based composite coatings with embedded lubricant particles from an additive-free Watts bath. In this sense, whereas the combination of ultrasound with mechanical agitation was the best method to disperse the lubricant particles in the Watts bath, ultrasound on its own yielded the best composite coatings in terms of higher incorporation and uniform distribution of finely dispersed particles within the Ni coatings, highlighting the importance of setting the best operational conditions for each stage of the electrodeposition process.

Regarding those Ni/WS_2 and Ni/hBN composite coatings that exhibit a better quality in terms of particle incorporation and distribution (both electrodeposited under ultrasound at 0.180 W/cm^3), the particle content in Ni/WS_2 composite coatings was around five times greater than in the Ni/hBN composite coatings. Ni/WS_2 composite coatings also presented a more significant change in crystal orientation, surface morphology, crystal structure and grain size. This grain refinement effect would be the main cause for the significant increase in hardness here reported. Current efforts are being put into the investigation of the tribological performance of the novel Ni/WS_2 composite coatings electrodeposited from an additive-free Watts bath under ultrasound, as these coatings constitute a good candidate for replacing current electrodeposited Ni coatings in different industrial applications.

ACKNOWLEDGMENTS

The authors acknowledge TSB and EPSRC in UK for their funding through the KTP scheme. The authors also thank Dr M.L. Wears from the University of Exeter and Dr G. West from Loughborough University for their assistance with XRD and FIB-SEM analysis, respectively. The authors would also like to acknowledge the contribution of Prof. A. Bund and Dr M. Camargo from Technische Universität Ilmenau for the GD-OES data here included, and Dr R. Griesler, also from Technische Universität Ilmenau, for the insightful discussions on XRD analysis and crystal orientation.

TABLES

Table 1. Ni Watts process and particles used in the present study.

Bath composition	
$NiSO_4.6H_2O$	290 g/L
$NiCl_2.6H_2O$	50 g/L
H_3BO_3	30 g/L
Particles	
Types	WS_2 (D50* ≈ 0.6μm, D90** ≈ 5μm) hBN (D50 ≈ 0.5μm, D90 ≈ 1.1μm)
Concentration	15 g/L
Plating conditions	
pH	3.2
Temperature	50 ºC
Current density	4 A/dm^2

* D50 is the median particle size provided by the supplier, meaning that 50% of the particles are smaller than the said size.

**D90 is the 90th percentile of the particle size provided by the supplier, meaning that 90% of the particles are smaller than said size.

FIGURES

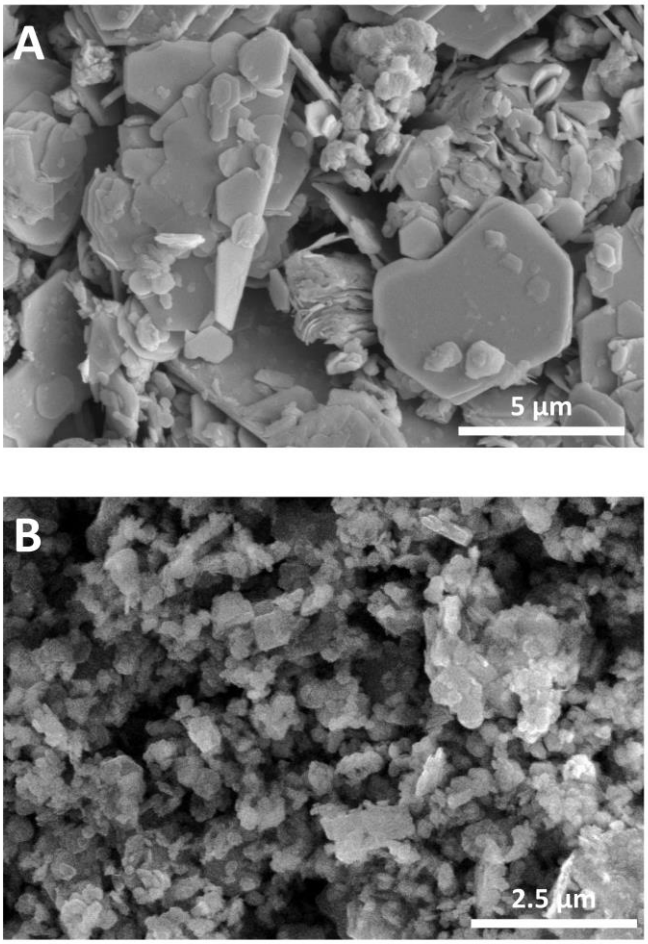

Figure 1. SEM images of the different lubricant particles used in the present research project: A) WS_2, B) hBN.

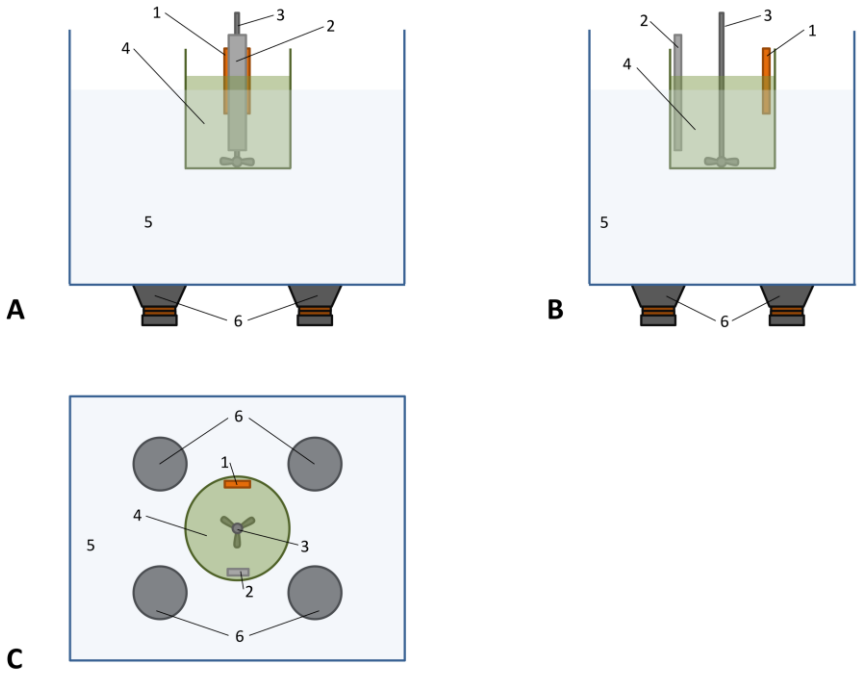

Figure 2. Diagram showing front (A), lateral (B) and top (C) views of the experimental set-up used in the present study. Numbered elements are: 1) Cu cathode, 2) Ni anode, 3) overhead stirrer (when required), 4) 600 mL beaker containing 500 mL of Watts bath, 5) ultrasonic bath, and 6) ultrasonic transducers.

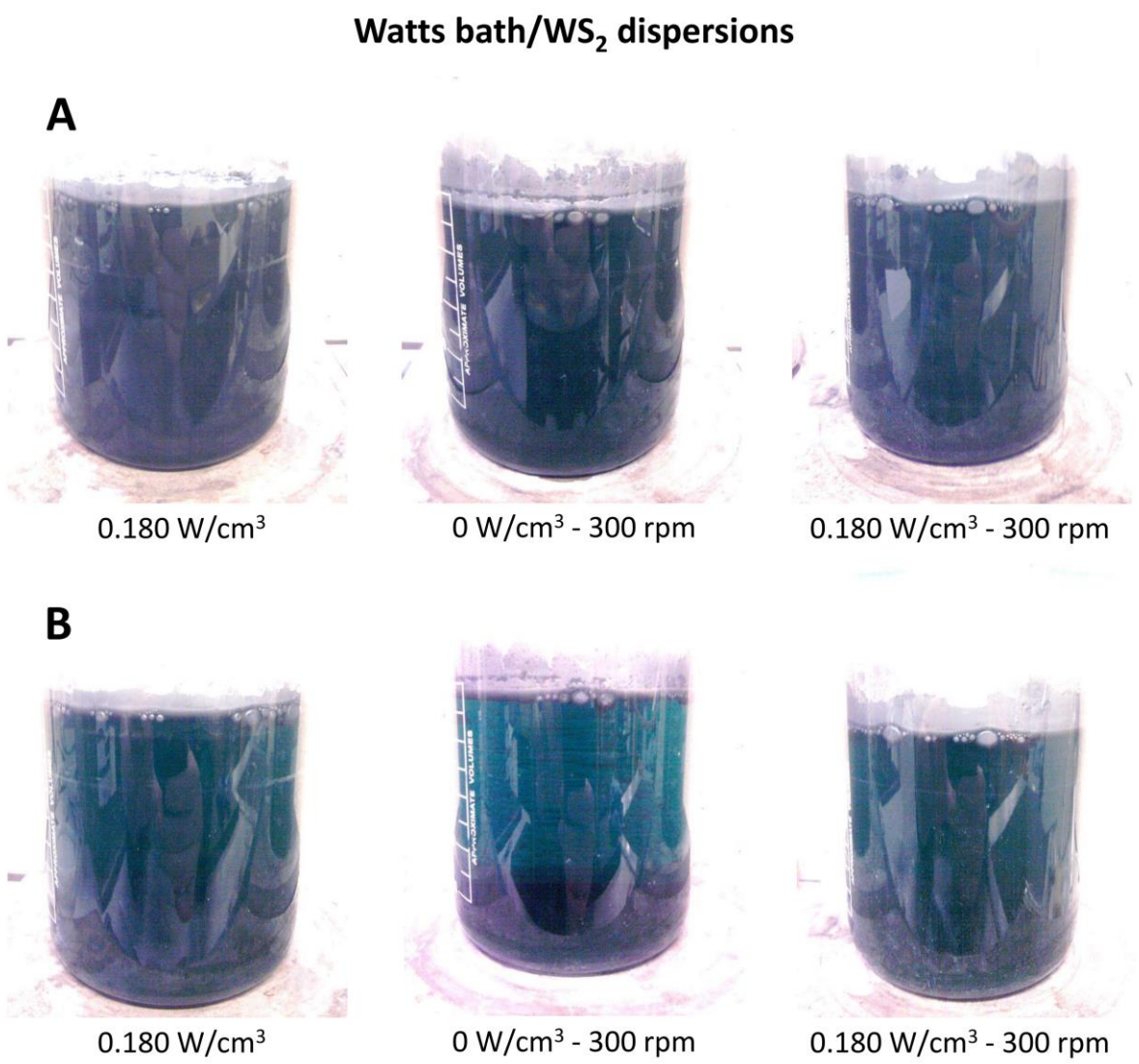

Figure 3. Appearance of Watts bath/WS_2 dispersions: A) immediately after dispersing the particles and B) 60 minutes after dispersing the particles. In all cases, the WS_2 particles were dispersed for 30 minutes in the electrolyte by different dispersing methods. Images were edited (50% increase in brightness) to show the quality of the dispersion. (For better visualization of images in colour, the reader is referred to the web version of this article.)

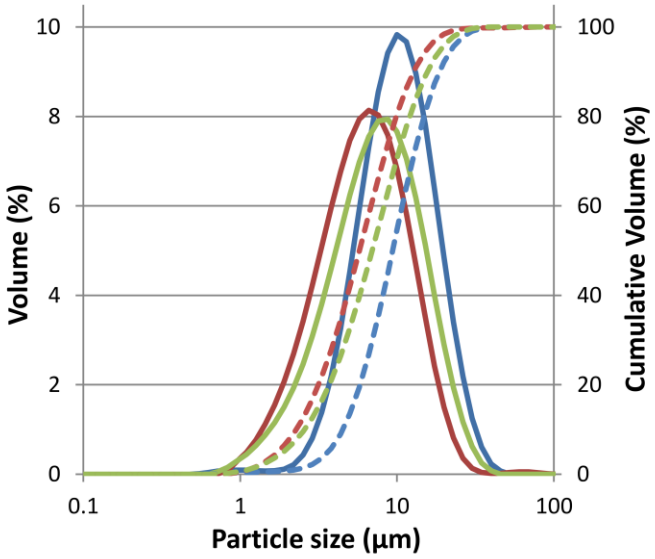

Figure 4. Particle size distribution curves (solid line: particle size distribution, dashed line: accumulated particle size distribution) obtained from experiments conducted in diluted Watts bath/WS_2 dispersions prepared by different dispersing methods: ultrasound at 0.180 W/cm^3 (green lines), mechanical agitation at 300 rpm (blue lines) and combined ultrasound/mechanical agitation at 0.180 W/cm^3 – 300 rpm (red lines). (For interpretation of the references in colour in this figure legend, the reader is referred to the web version of this article.)

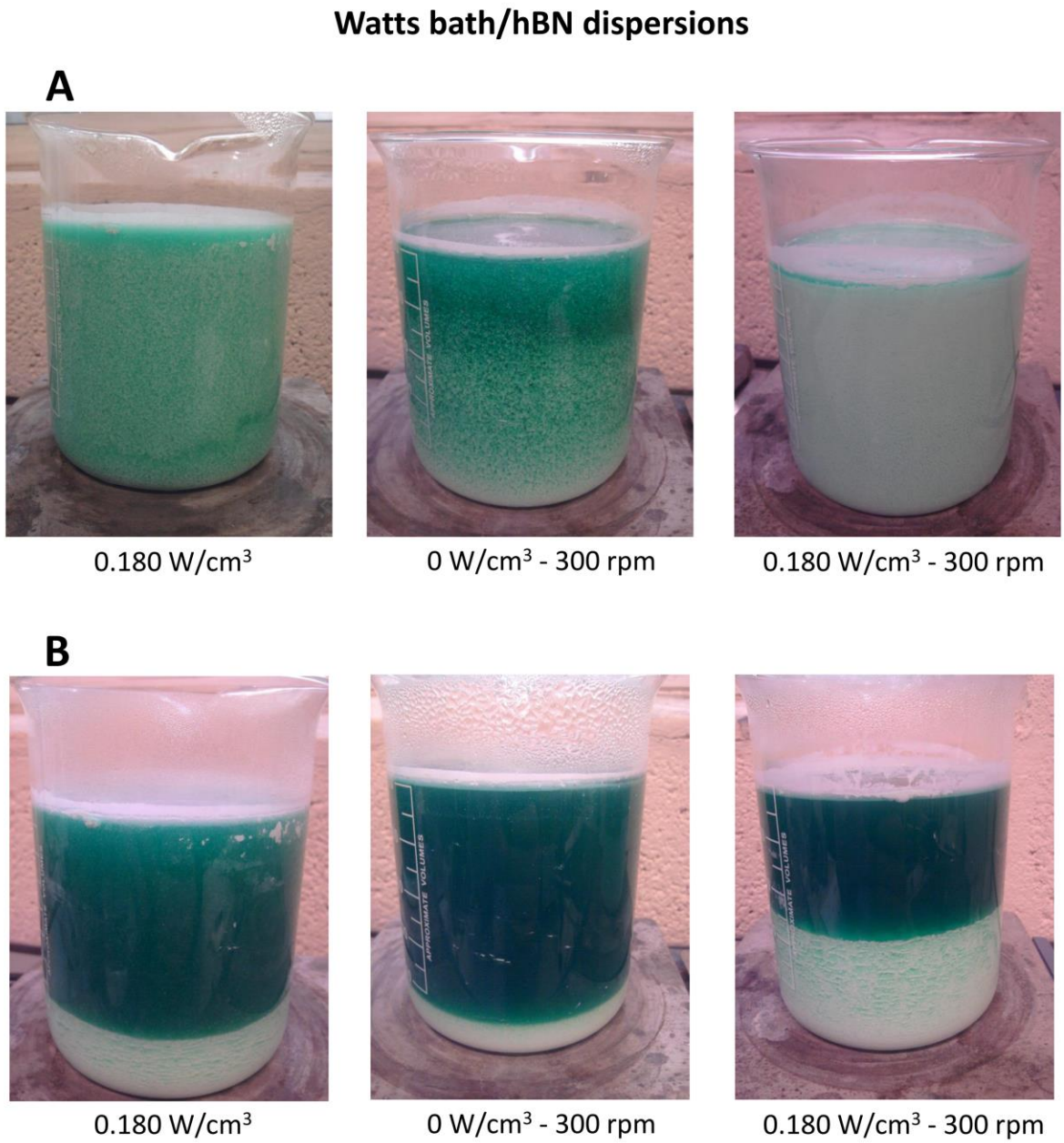

Figure 5. Appearance of Watts bath/hBN dispersions: A) immediately after dispersing the particles and B) 60 minutes after dispersing the particles. In all cases, the hBN particles were dispersed for 30 minutes in the electrolyte by different dispersing methods. Images were edited (50% increase in brightness) to show the quality of the dispersion. (For better visualization of images in colour, the reader is referred to the web version of this article.)

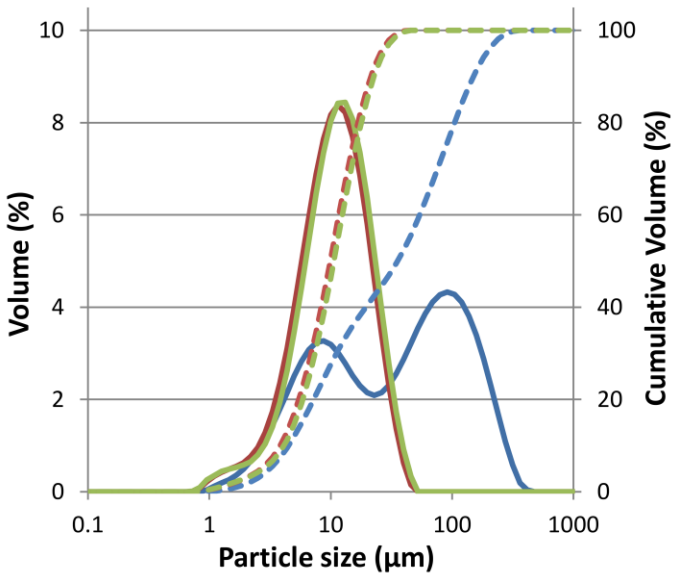

Figure 6. Particle size distribution curves (solid line: particle size distribution, dashed line: accumulated particle size distribution) obtained from experiments conducted in diluted Watts bath/hBN dispersions prepared by different dispersing methods: ultrasound at 0.180 W/cm^3 (green lines), mechanical agitation at 300 rpm (blue lines) and combined ultrasound/mechanical agitation at 0.180 W/cm^3 – 300 rpm (red lines). (For interpretation of the references in colour in this figure legend, the reader is referred to the web version of this article.)

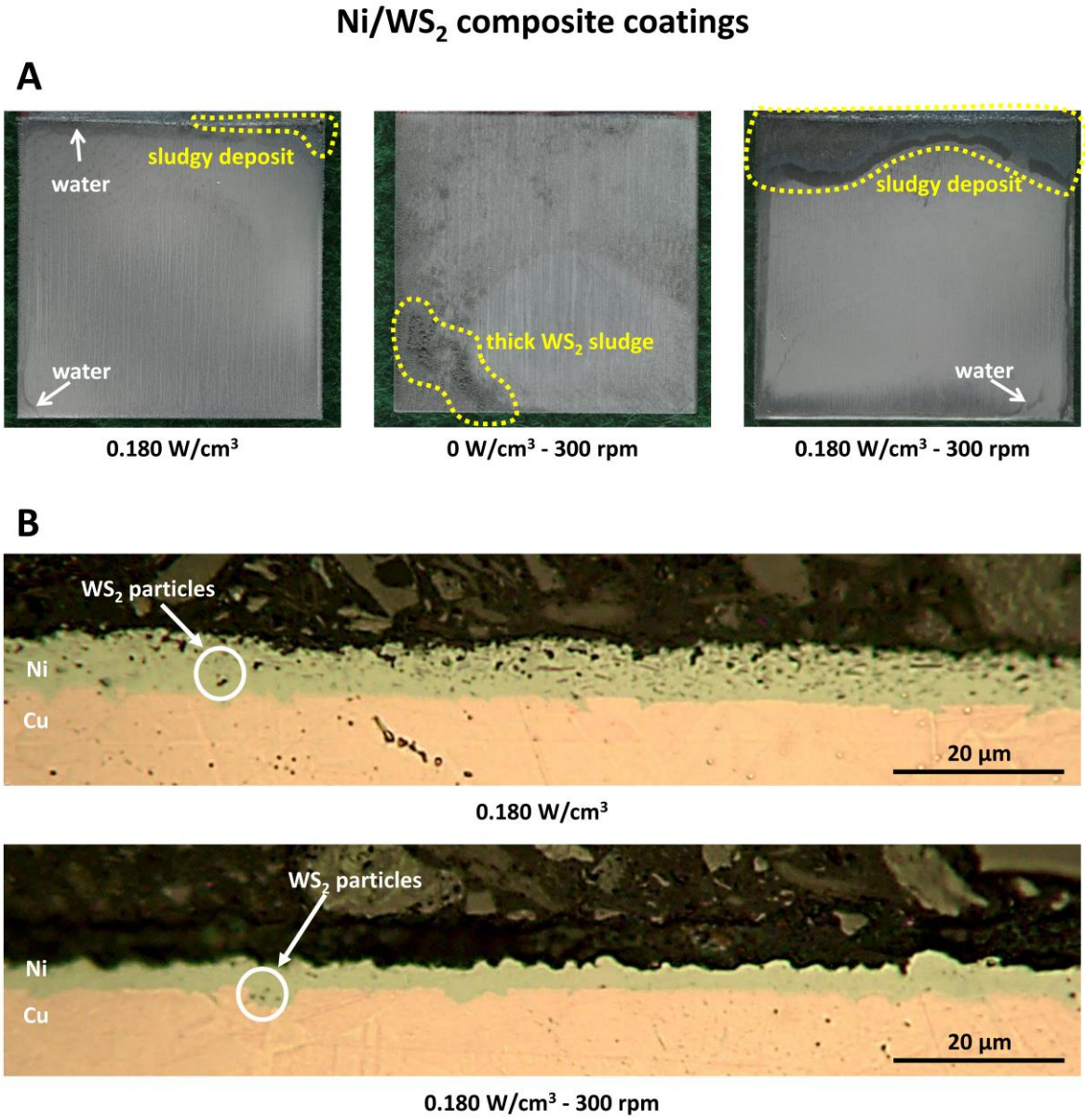

Figure 7. A) Surface finish of Ni/WS_2 composite coatings electrodeposited under ultrasound at 0.180 W/cm^3, mechanical agitation at 300 rpm and combined ultrasound/mechanical agitation at 0.180 W/cm^3 – 300 rpm. Moisture (water) stains can be seen near the edges in some of the samples. Electrodeposition time: 14 minutes. Current density: 4 A/dm^2. B) Cross-section images of Ni/WS_2 composite coatings electrodeposited under ultrasound at 0.180 W/cm^3 and combined ultrasound/mechanical agitation at 0.180 W/cm^3 – 300 rpm. Electrodeposition time: 14 minutes. Current density: 4 A/dm^2. (For better visualization of images in colour, the reader is referred to the web version of this article.)

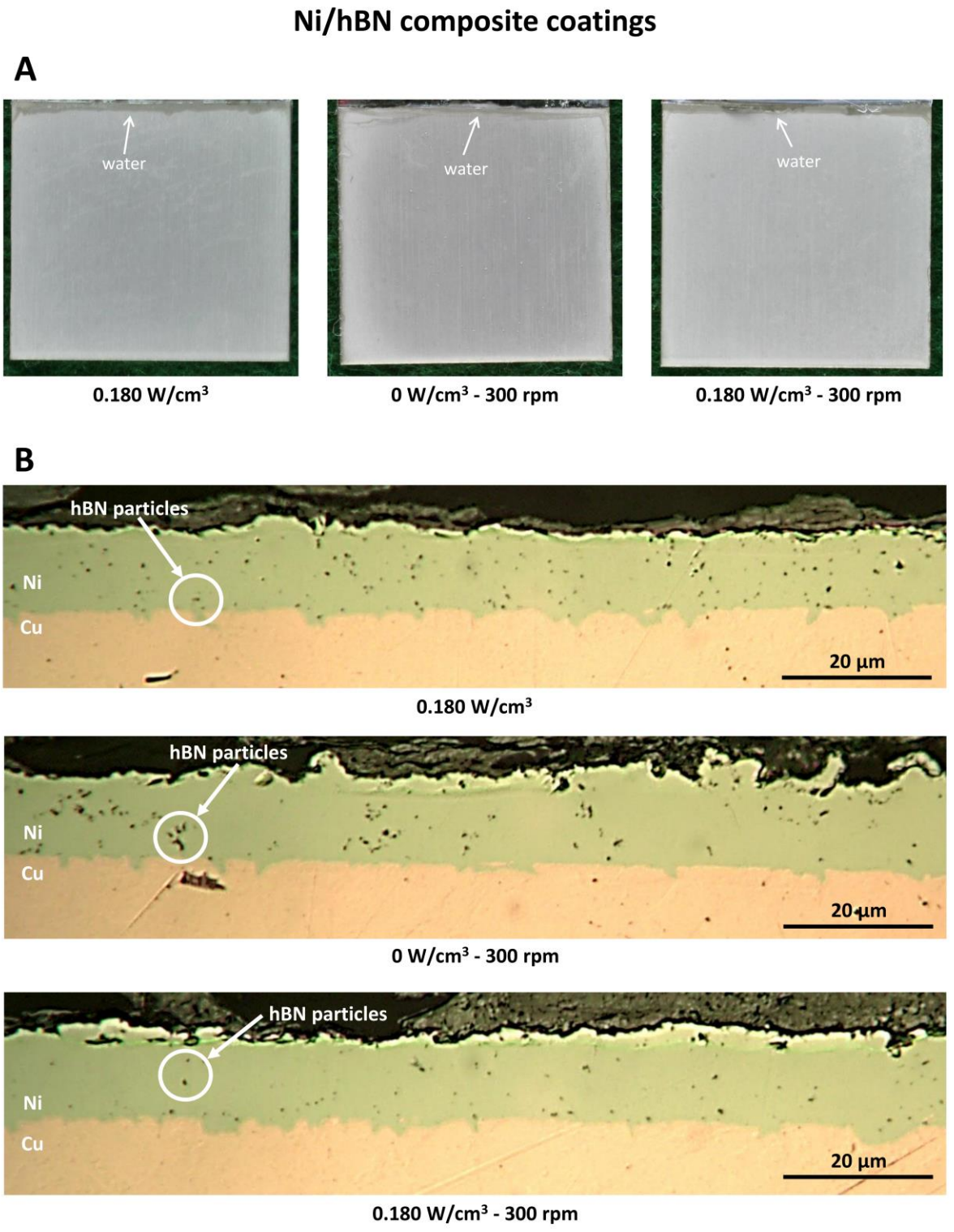

Figure 8. A) Surface finish of Ni/hBN composite coatings electrodeposited under ultrasound at 0.180 W/cm^3, mechanical agitation at 300 rpm and combined ultrasound/mechanical agitation at 0.180 W/cm^3 – 300 rpm. Moisture (water) stains can be seen near upper edges of the samples. Electrodeposition time: 14 minutes. Current density: 4 A/dm^2. B) Cross-section images of Ni/hBN composite coatings electrodeposited under ultrasound at 0.180 W/cm^3, mechanical agitation at 300 rpm and combined ultrasound/mechanical agitation at 0.180 W/cm^3 – 300 rpm. Coatings shown here were electrodeposited for longer times (24 minutes) in order to

achieve thicker coatings for easier observation of the particles. Current density: 4 A/dm². (For better visualization of images in colour, the reader is referred to the web version of this article.)

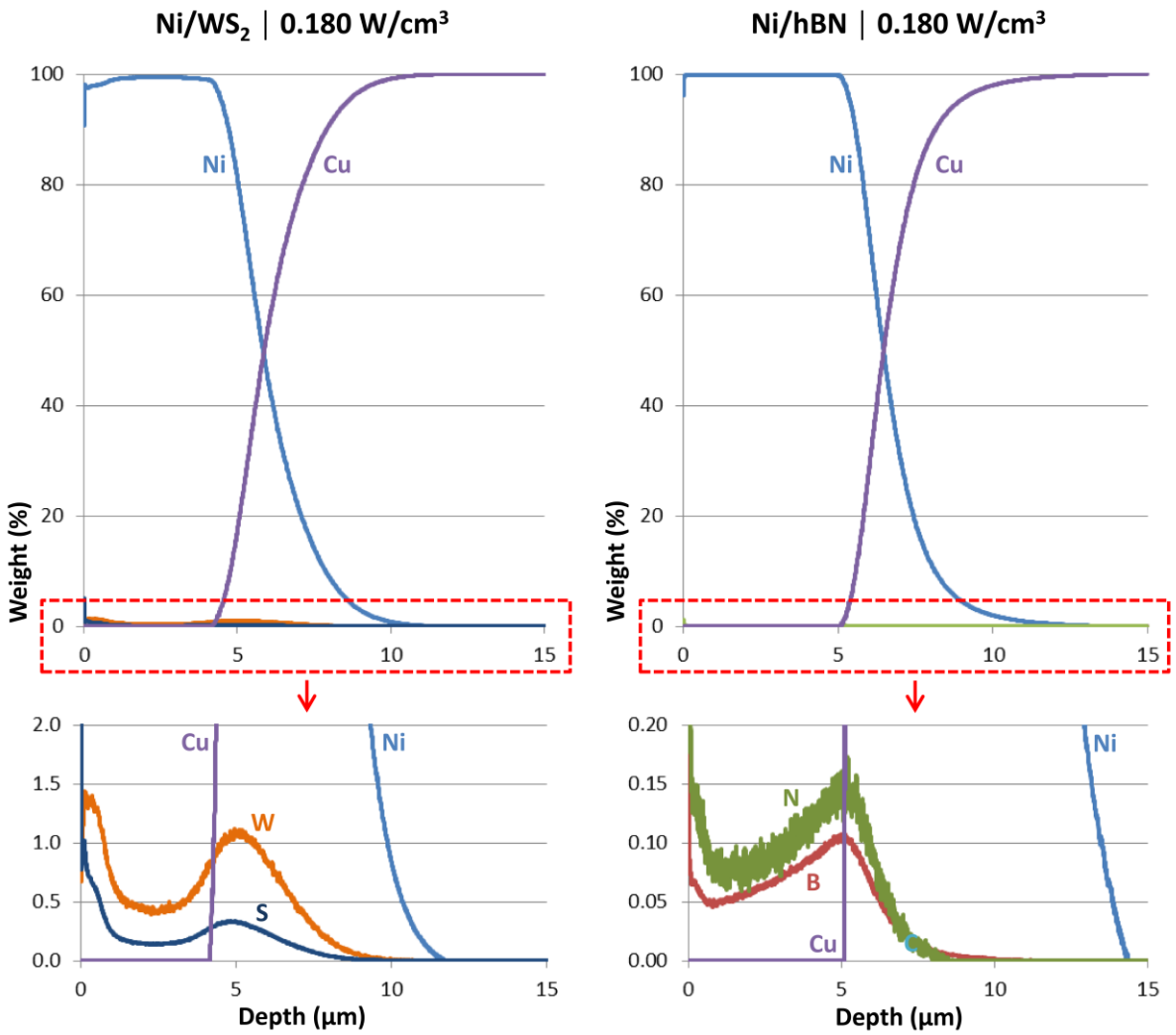

Figure 9. GD-OES depth profiles of the presence of different atoms (Ni, Cu, W, S, B, and N) in a Ni/WS_2 composite coating (left) and a Ni/hBN composite coating (right) electrodeposited under ultrasound. (For interpretation of the references in colour in this figure legend, the reader is referred to the web version of this article.)

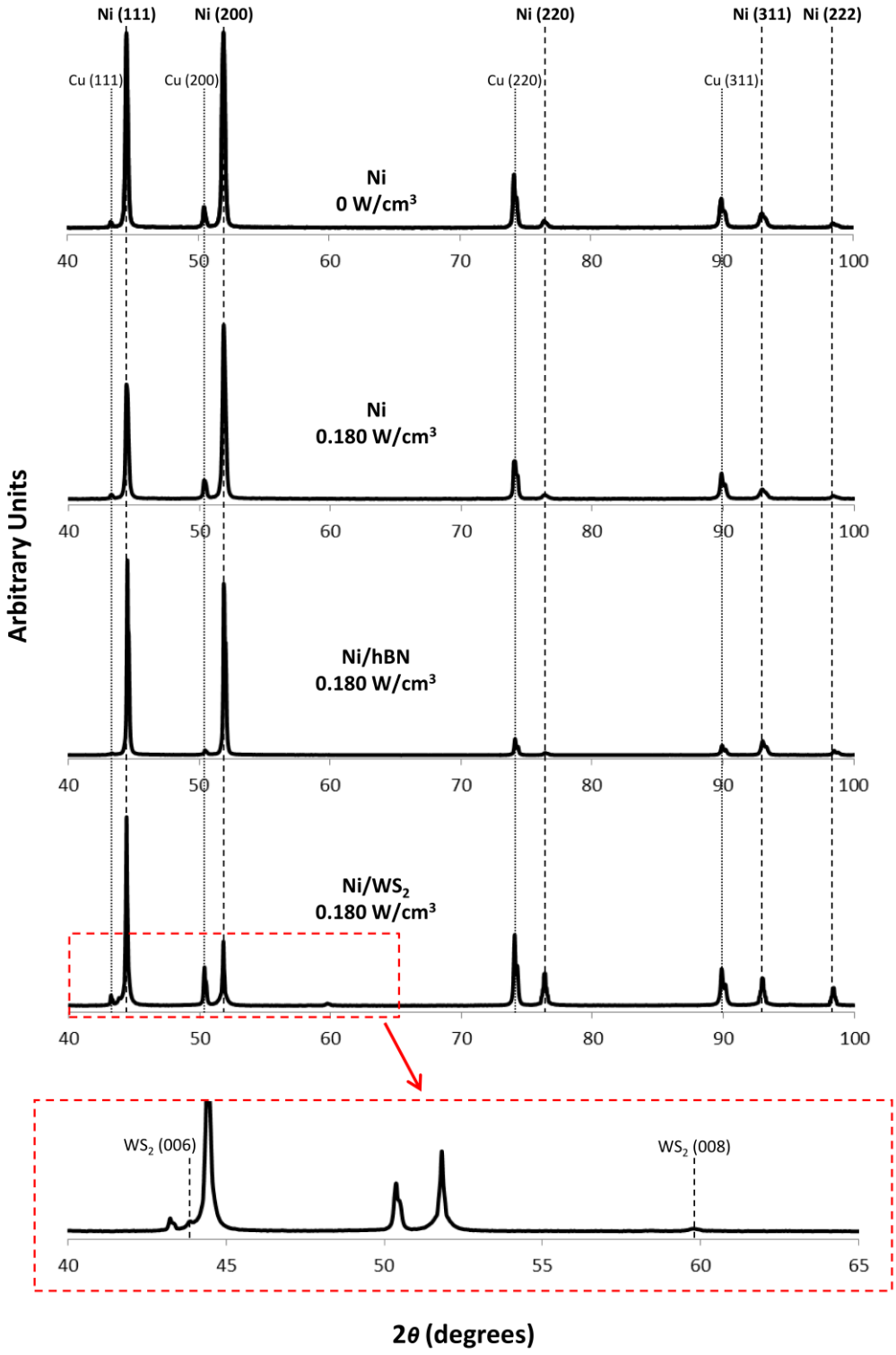

Figure 10. XRD spectra of Ni/WS_2 and Ni/hBN composite coatings electrodeposited under ultrasound at 0.180 W/cm^3. XRD spectra for pure Ni coatings electrodeposited under silent/still conditions and ultrasound at 0.180 W/cm^3 [14] are included for comparison purposes. Zoomed-in area: XRD spectra of the Ni/WS_2 composite where (006) and (008) crystal planes associated to the presence of WS_2 are highlighted.

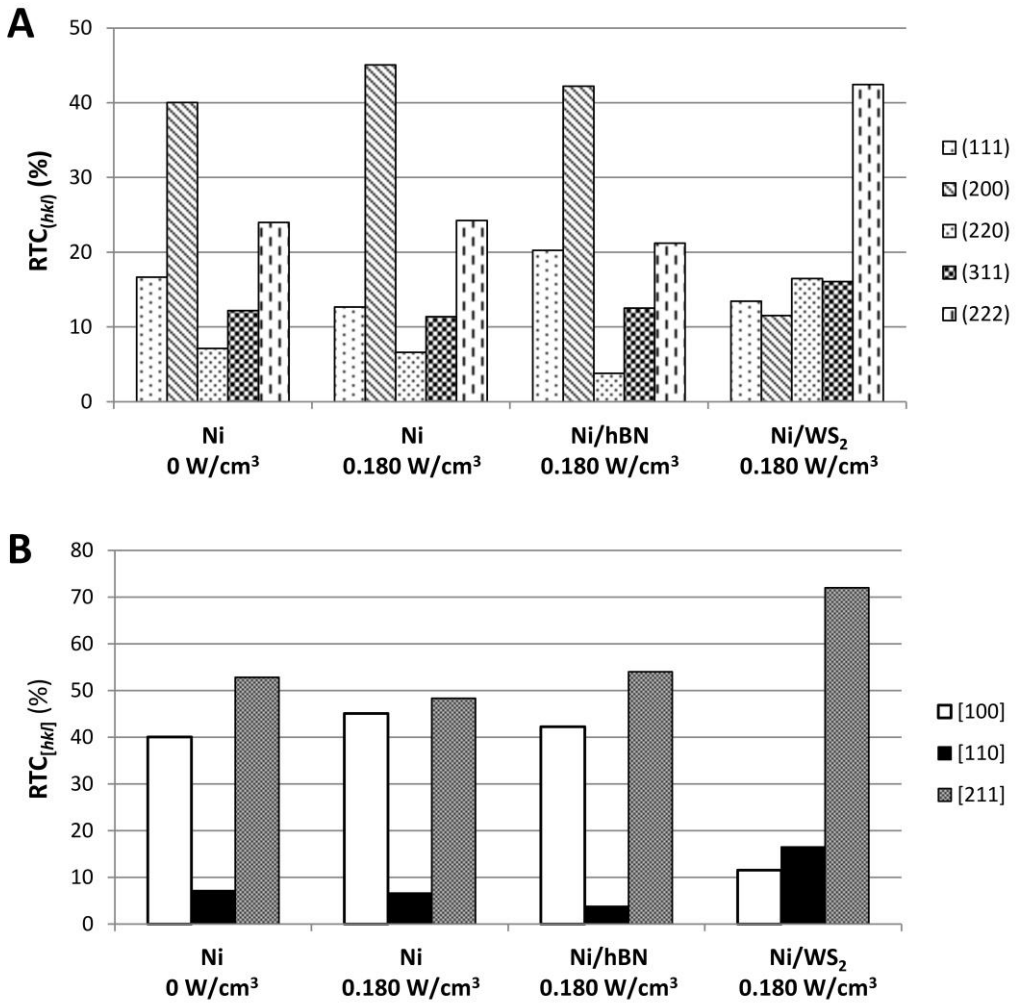

Figure 11. A) $RTC_{(hkl)}$ estimated for (111), (200), (311) and (222) crystal planes and B) $RTC_{[hkl]}$ estimated for [100], [110], and [211] orientations observed in Ni/hBN and Ni/WS_2 coatings electrodeposited under ultrasound at 0.180 W/cm³. $RTC_{(hkl)}$ and $RTC_{[hkl]}$ corresponding to pure Ni coatings electrodeposited under silent/still conditions and ultrasound at 0.180 W/cm³ [14] are included for comparison purposes.

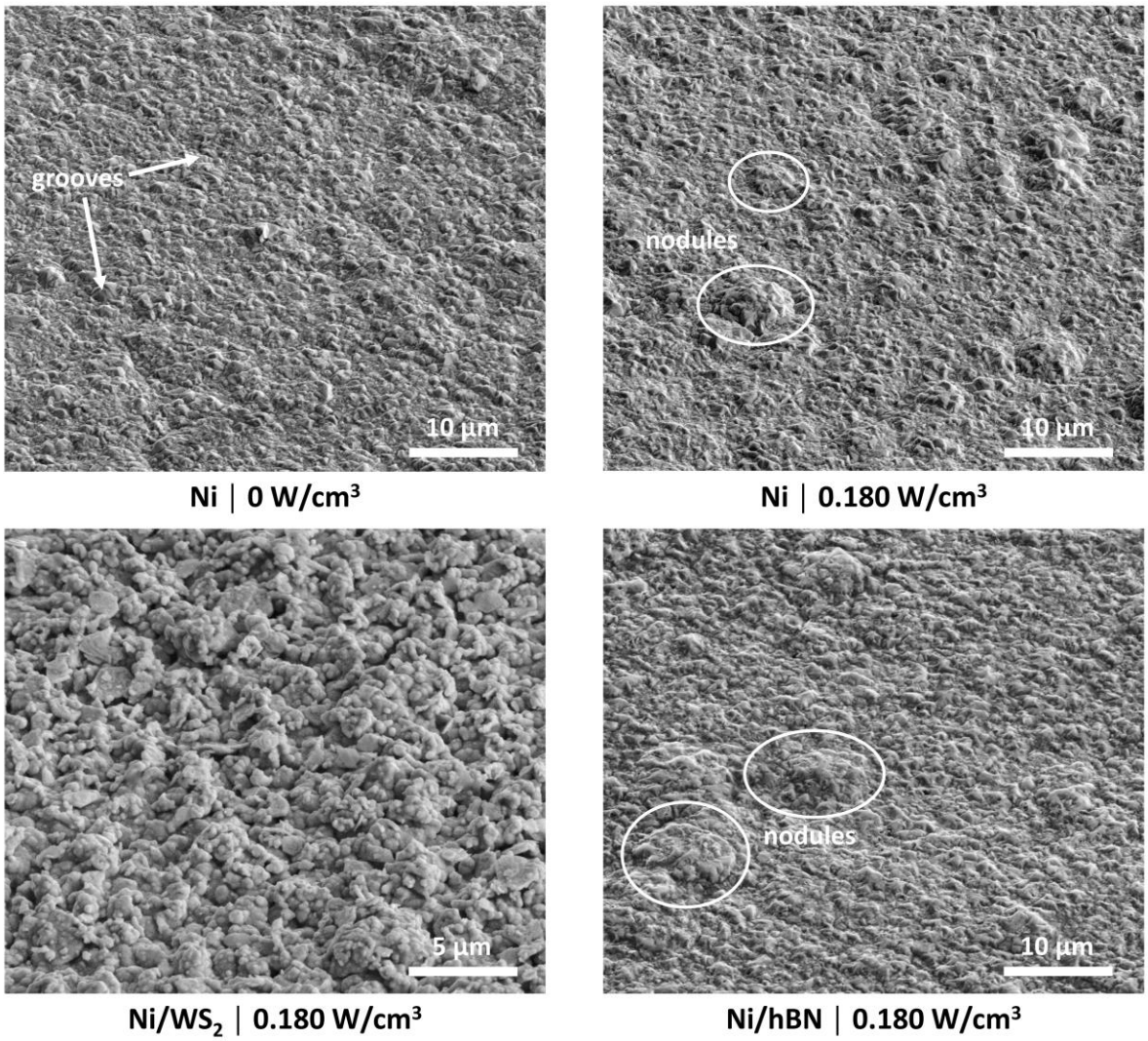

Figure 12. Tilted FIB-SEM images of the surface of Ni/WS_2 and Ni/hBN composite coatings electrodeposited under ultrasound at 0.180 W/cm^3. Tilted FIB-SEM images corresponding to pure Ni coatings electrodeposited under silent/still conditions and ultrasound at 0.180 W/cm^3 [14] are included for comparison purposes.

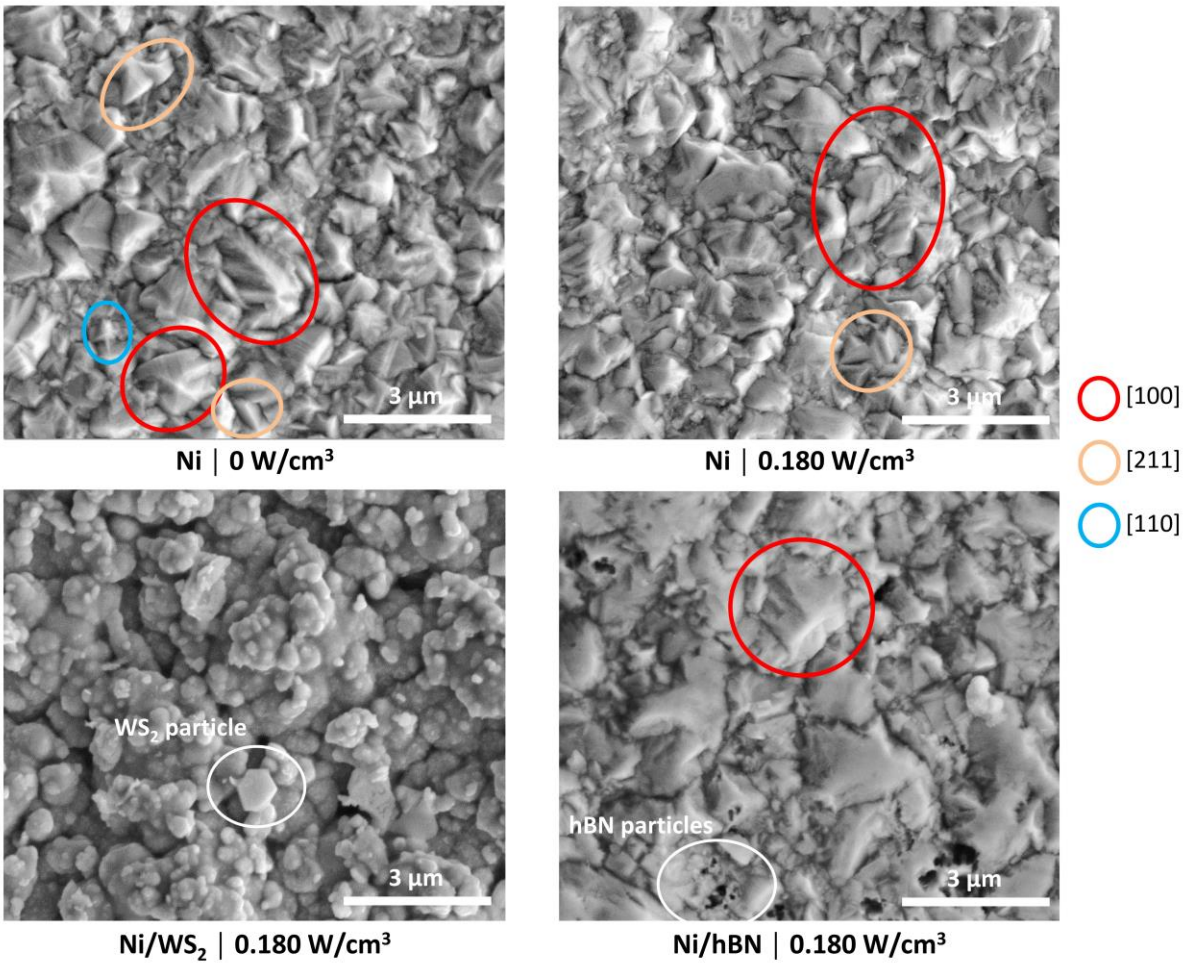

Figure 13. High magnification FIB-SEM images of the surface of Ni/WS_2 and Ni/hBN composite coatings electrodeposited under ultrasound at 0.180 W/cm³. High magnification FIB-SEM images corresponding to pure Ni coatings electrodeposited under silent/still conditions and ultrasound at 0.180 W/cm³ [14] are included for comparison purposes. (For interpretation of the references in colour in this figure legend, the reader is referred to the web version of this article.)

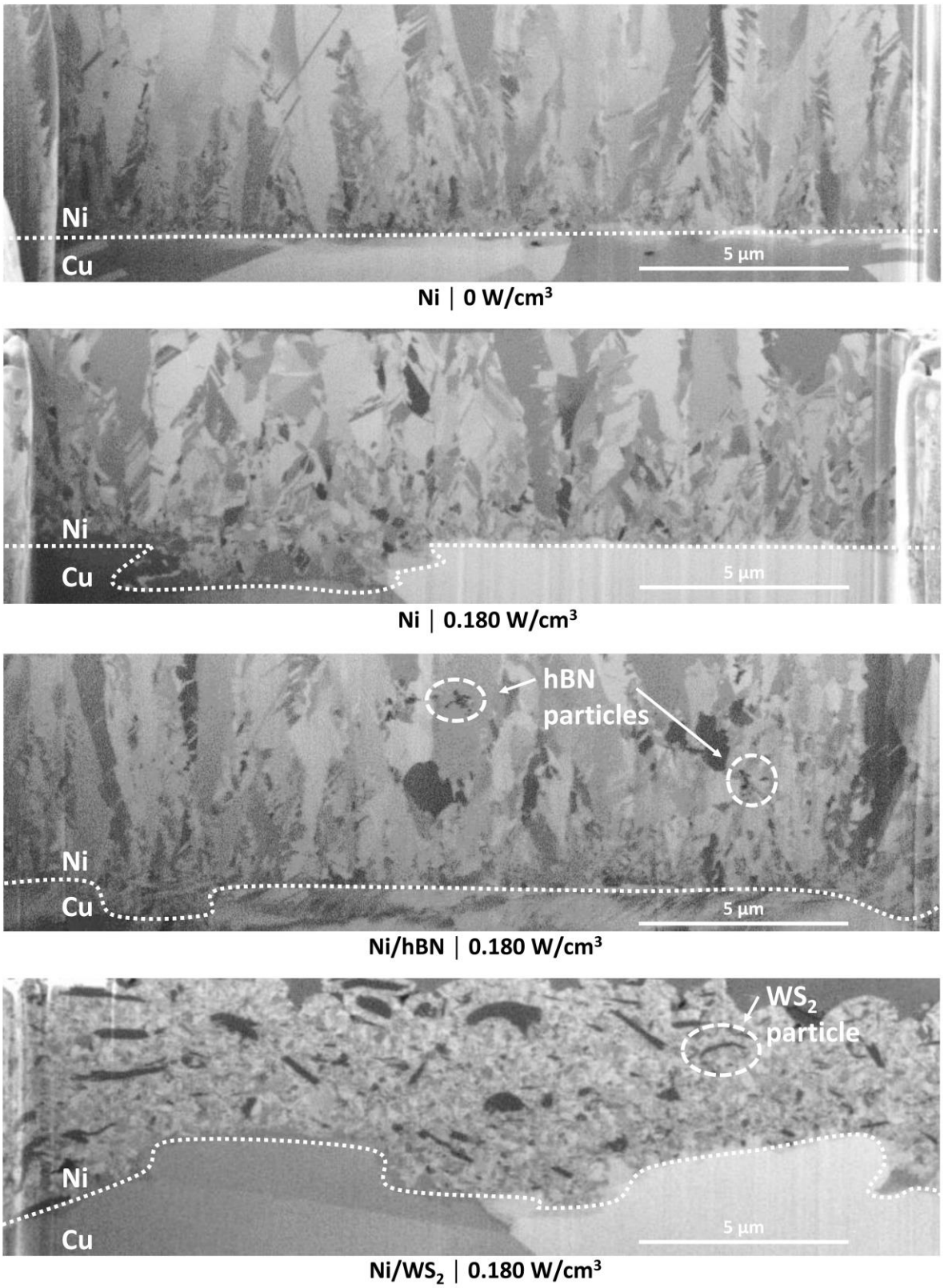

Figure 14. FIB-SEM images of the cross-section of Ni/WS_2 and Ni/hBN composite coatings electrodeposited under ultrasound at 0.180 W/cm^3. FIB-SEM images of the cross-section of pure Ni coatings electrodeposited under silent/still conditions and ultrasound at 0.180 W/cm^3 [14] are included for comparison purposes.

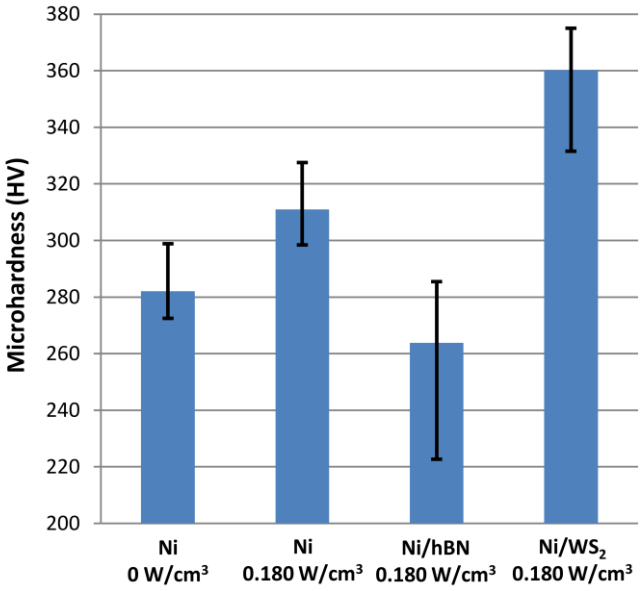

Figure 15. Microhardness values measured in the central area of Ni/hBN and Ni/WS_2 composite coatings electrodeposited under ultrasound at 0.180 W/cm³. Microhardness values measured on pure Ni coatings electrodeposited under silent/still conditions and ultrasound at 0.180 W/cm³ [14] are included for comparison purposes.

REFERENCES

[1] C.T.J. Low, R.G.A. Wills, F.C. Walsh, Surf. Coat. Technol. 201 (2006) 371-383.

[2] M. Lekka, N. Kouloumbi, M. Gajo, P.L. Bonora, Electrochim. Acta 50 (2005) 4551-4556.

[3] S.T. Aruna, C.N. Bindu, V.E. Selvi, V.K.W. Grips, K.S. Rajam, Surf. Coat. Technol. 200 (2006) 6871-6880.

[4] S.A. Lajevardi, T. Shahrabi, Appl. Surf. Sci. 256 (2010) 6775-6781.

[5] C.T.J. Low, J.O. Bello, J.A. Wharton, R.J.K. Wood, K.R. Stokes, F.C. Walsh, Surf. Coat. Technol. 205 (2010) 1856-1863.

[6] P. Bercot, E. Peña-Muñoz, J. Pagetti, Surf. Coat. Technol. 157 (2002) 282-289.

[7] E. Pompei, L. Magagnin, N. Lecis, P.L. Cavallotti, Electrochim. Acta 54 (2009) 2571-2574.

[8] Ali Erdemir, Solid lubricants and self-lubricating films, in: B. Bhushan (Ed.), Modern Tribology Handbook, CRC Press, Boca Raton-London-New York-Washington D.C., 2000.

[9] I. Tudela, Y. Zhang, M. Pal, I. Kerr, A.J. Cobley, Surf. Coat. Technol. 259 (2014) 363-373.

[10] E. García-Lecina, I. García-Urrutia, J.A. Díez, J. Morgiel, P. Indyka, Surf. Coat. Technol. 206 (2012) 2998-3005.

[11] C. Zanella, M. Lekka, P.L. Bonora, Surf. Eng. 26 (2010) 511-518.

[12] F.-f. Xia, M.-h.Wu, F. Wang, Z.-y. Jia, A.-l. Wang, Curr. Appl. Phys. 9 (2009) 44-47.

[13] E. García-Lecina, I. García-Urrutia, J.A. Díez, J. Fornell, E. Pellicer, J. Sort, Electrochim. Acta 114 (2013) 859-867.

[14] I. Tudela, Y. Zhang, M. Pal, I. Kerr, T.J. Mason, A.J. Cobley, Surf. Coat. Technol. 264 (2015) 49-59.

[15] T.J. Mason, Practical Sonochemistry: User's Guide to Applications in Chemistry and Chemical Engineering, Ellis Horword Ltd., Chichester, 1991.

[16] Ratoarinoro, F. Contamine, A.M. Wilhelm, J. Berlan, H. Delmas, Ultrason. Sonochem. 2 (1995) S43-S47.

[17] O. Louisnard, J. González-García, in: H. Feng, G. Barbosa-Canovas, J.Weiss (Eds.), Ultrasound Technologies for Food and Bioprocessing, Springer, New York-Dordrecht-Heidelberg-London, 2011.

[18] P. Indyka, E. Beltowska-Lehman, M. Bieda, J. Morgiel, L. Tarkowski, Solid State Phenom. 186 (2012) 234-238.

[19] E. Beltowska-Lehman, P. Indyka, A. Bigos, M. Kot, L. Tarkowski, Surf. Coat. Technol. 211 (2012) 62–64.

[20] D.P. Weston, Y.Q. Zhu, D. Zhang, C. Miller, D.G. Kingerley, C. Carpenter, S.J. Harris, N.J. Weston, Electrochim. Acta 56 (2011) 6837-6846.

[21] H.-Y. Zheng, M.-Z. An, J. Alloys Compd. 459 (2008) 548-552.

[22] O. Louisnard, Ultrason. Sonochem. 19 (2012) 56-65.

[23] O. Louisnard, Ultrason. Sonochem. 19 (2012) 66-76.

[24] T. Wriedt, Mie theory: A review, in: W. Hergert, T. Wriedt (Eds.), The Mie Theory, Springer Series in Optical Sciences 169, Springer-Verlag, Berlin-Heidelberg, 2012.

[25] T. Hielscher, Ultrasonic production of nano-size dispersions and emulsions, European Nano Systems 2005, 2005. (Paris, France, 14-16 December).

[26] S. Alfihed, M. Hossain, A. Alharbi, A. Alyamani, F.H. Alharbi, J. Mater. 2013 (2013) 603648.

[27] Ioffe Physical Technical Institute of Russia, New Semiconductor Materials: Characteristics and Properties Database, BN – Boron Nitride.
http://www.ioffe.rssi.ru/SVA/NSM/Semicond/BN/basic.html#hexagonal

[28] G. Eshel, G.J. Levy, U. Mingelgrin, M. J. Singer, Soil Sci. Soc. Am. J. 68 (2004) 736.

[29] C. Murphy, Nanoparticle Sizing – Think of a number, Nanotechnology and the Coatings Industry 2012, 2012. (Nottingham, United Kingdom, 8 October).

[30] S. Alfihed, M. Hossain, A. Alharbi, A. Alyamani, F.H. Alharbi, J. Mater. 2013 (2013) 603648.

[31] E. Kissa, Dispersions Characterization, Testing and Measurement, Marcel Dekker, New York, 1999.

[32] E.J. Podlaha, Nano Lett. 1 (2001) 413-416.

[33] R.N. Kelly, F.M. Etzler, What is wrong with laser diffraction? - A critical review of current laser diffraction methods for particle size analysis. http://www.donner-tech.com/whats_wrong_with_ld.pdf

[34] M.-D. Ger, Mater. Chem. Phys. (87) 67-74.

[35] J. Fransaer, J.-P. Celis, J. R. Roos, J. Electrochem. Soc. 139 (1992) 413-425.

[36] I. García, J. Fransaer, J.-P. Celis, Surf. Coat. Technol. 148 (2001) 171-178.

[37] D. Alberts, B. Fernández, T. Frade, A. Gomes, M.I. da Silva Pereira, R. Pereiro, A. Sanz-Medel, Talanta 84 (2011) 572-578.

[38] M. Camargo, I. Díaz, U. Schmidt, A. Bund, Galvanotechnik 103 (2012) 48-56.

[39] M. Camargo, U. Schmidt, R. Grieseler, M. Wilke, A. Bund, J. Electrochem. Soc. 161 (2014) D168-D175.

[40] L. Ph. Bérubé, G. L'Espérance, J. Electrochem. Soc. 136 (1989) 2314-2315.

[41] S. Surviliene, V. Jasulaitiene, A. Lisowska-Oleksiak, V. A. Safonov, J. Appl. Electrochem. 35 (2005) 9-15.

[42] E.A. Pavlatou, N. Spyrellis, Russ. J. Electrochem. 44 (2008) 745-754.

[43] S. Spanou, E.A. Pavlatou, N. Spyrellis, Electrochim. Acta 54 (2009) 2547-2555.

[44] C.N. Panagopoulos, E.P. Georgiou, A. Tsopani, L. Piperi, Appl. Surf. Sci. 257 (2011) 4769-4773.

[45] Inorganic Crystal Structure Database code 64989, Fachinformationszentrum Karlsruhe (Germany) and National Institute of Standards and Technology (United States of America).

[46] J. Amblard, M. Froment, G. Maurin, Electrodepos. Surf. Treat. 2 (1974) 205-222.

[47] E.A. Pavlatou, M. Raptakis, N. Spyrellis, Surf. Coat. Technol. 201 (2007) 4571-4577.

[48] S. Spanou, E.A. Pavlatou, J. Appl. Electrochem. 40 (2010) 1325-1336.

[49] J. Amblard, M. Froment, N. Spyrellis, Surf. Technol. 5 (1977) 205-234.

[50] J. Amblard, M. Froment, Faraday Symp. Chem. Soc. 12 (1977) 136-144.

[51] J. Amblard, I. Epelboin, M. Froment, G. Maurin, J. Appl. Electrochem. 9 (1979) 233-242.

[52] J. Amblard, M. Froment, G. Maurin, N. Spyrellis, E. Trevisan-Souteyrand, Electrochim. Acta 28 (1983) 909-915.

[53] A.G. McCormack, M.J. Pomeroy, V.J. Cunnane, J. Electrochem. Soc. 150 (2003) C356-C361.

[54] E.A. Pavlatou, M. Stroumbouli, P. Gyftou, N. Spyrellis, J. Appl. Electrochem. 36 (2006) 385-394.

[55] E. García-Lecina, I. García-Urrutia, J.A. Díez, M. Salvo, F. Smeacetto, G. Gautier, R. Seddon, R. Martin, Electrochim. Acta 54 (2009) 2556-2562.

[56] S. Özkan, G. Hapçı, G. Orhan, K. Kazmanlı, Surf. Coat. Technol. 232 (2013) 734-741.

[57] H. Gül, F. Kiliç, S. Aslan, A. Alp, H. Akbulut, Wear 267 (2009) 976-990.

[58] A. Vicenzo, P.L. Cavalloti, Russ. J. Electrochem. 44 (2008) 716-727.

[59] J. Kubisztal, A. Budniok, A. Lasia, Int. J. Hydrogen Energ. 32 (2007) 1211-1218.

[60] S. Mohajeri, A. Dolati, S. Rezagholibeiki, Mater. Chem. Phys. 129 (2011) 746-750.

[61] M. Lekka, D. Koumoulis, N. Kouloumbi, P.L. Bonora, Electrochim. Acta 54 (2009) 2540-2546.

[62] C. Cai, X.B. Zhu, G.Q. Zheng, Y.N. Yuan, X.Q. Huang, F.H. Cao, J.F. Yang, Z. Zhang, Surf. Coat. Technol. 205 (2011) 3448-3454.

[63] P. Scherrer, Bestimmung der Größe und der inneren Struktur von Kolloidteilchen mittels Röntgenstrahlen, in: Nachrichten von der Gesellschaft der Wissenschaften zu Göttingen, Mathematisch-Physikalische Klasse, 1918, pp 98-100.

[64] T. Lampke, D. Dietrich, A. Leopold, G. Alisch, B. Wielage, Surf. Coat. Technol. 202 (2008) 3967-3974.

[65] C.T. Walker, R. Walker, Electrodepos. Surf. Treat. 1 (1973) 457-469.

[66] D.H. Jeong, F. Gonzalez, G. Palumbo, K.T. Aust, U. Erb, Scripta Mater. 44 (2001) 493-499.

[67] Y.-J. Xue, J.-S. Li, W. Ma, M.-D. Duan, M.-M. Lan, Int. J. Surf. Sci. Eng. 4 (2010) 202-213.

[68] Q. Feng, T. Li, H. Yue, K. Qi, F. Bai, J. Jin, Appl. Surf. Sci. 254 (2008) 2262-2268.

[69] C. Zanella, M. Lekka, P.L. Bonora, Surf. Eng. 26 (2010) 511-518.

[70] S. A. Lajevardi, T. Shahrabi, V. Hasannaeimi, Mater. Corros. 62 (2011) 29-34.

[71] J. Li, Y. Sun, X. Sun, J. Qiao, Surf. Coat. Technol. 192 (2005) 331-335.

[72] I. Sivandipoor, F. Ashrafizadeh, Appl. Surf. Sci. 263 (2012) 314-319.

[73] R. Balaji, M. Pushpavanam, K.Y. Kumar, K. Subramanian, Surf. Coat. Technol. 201 (2006) 3205-3211.

[74] V.D. Stankovic, M. Gojo, Surf. Coat. Technol. 81 (1996) 225-232.